THESIS FOR THE DEGREE OF DOCTOR OF PHILOSOPHY

Sustainable conversion of strategic industrial wastes and biomass into activated carbons for CO_2 capture: mechanisms, material design, and adsorption performance

BARTOSZ DZIEJARSKI

Department of Environmental and Energy Sciences

Energy Technology Division

CHALMERS UNIVERSITY OF TECHNOLOGY

Faculty of Environmental Engineering

Department of Air Conditioning, Heating, Gas Engineering and Air Protection

WROCŁAW UNIVERSITY OF SCIENCE AND TECHNOLOGY

Gothenburg, Sweden; Wrocław, Poland, 2026

Sustainable conversion of strategic industrial wastes and biomass into activated carbons for CO_2 capture: mechanisms, material design, and adsorption performance

BARTOSZ DZIEJARSKI
ISBN: 978-91-8103-447-9
DOI: https://doi.org/10.63959/chalmers.dt/590

Doktorsavhandlingar vid Chalmers tekniska högskola
Ny serie nr: 5904
ISSN: 0346-718X

Department of Environmental and Energy Sciences
Chalmers University of Technology
SE-412 96 Gothenburg
Sweden
Telephone + 46 (0)31-772 1000

Department of Air Conditioning, Heating, Gas Engineering and Air Protection
Wrocław University of Science and Technology
ul. Norwida 4/6, 50-370 Wrocław
Poland

Cover:
Schematic illustration of the sustainable conversion of waste tires, lithium-ion batteries, and woody biomass into activated carbon as a gas sorbent for flue gas treatment, highlighting circular economy principles, waste valorization, and the adsorption of CO_2.

Printed by Chalmers Reproservice
Gothenburg, Sweden 2026

Abstract

The increasing concentration of atmospheric CO_2 necessitates sustainable sorbent materials for efficient carbon capture . This thesis explores the valorization of carbon-intensive waste streams into porous carbons for CO_2 capture within a circular materials framework. Three structurally distinct precursors were investigated: woody biomass, recovered carbon black from end-of-life tires, and graphite from spent lithium-ion batteries. Potassium-assisted chemical activation served as a unifying synthesis approach to establish structure–property–performance relationships and assess the chosen materials suitability as solid adsorbents.

The effects of precursor structure, activation conditions, and potassium speciation on pore development, carbon framework evolution, and surface chemistry were systematically analyzed. Particular attention was given to adsorption-relevant microporosity and its role in governing CO_2 uptake and CO_2/N_2 selectivity.

The obtained results suggested that activation responsiveness was strongly precursor-dependent. Biomass showed the highest reactivity toward KOH, yielding dense microporous networks with BET surface areas up to 2655 $m^2 g^{-1}$ and high CO_2 capacities, although excessive activation caused pore widening and performance loss. Recovered carbon black exhibited limited activation due to its compact morphology, leading to mesopore-dominated structures and lower uptake. Recovered graphite was the most resistant, with porosity developing mainly through defect-driven edge etching while preserving graphitic order.

CO_2 adsorption across all systems was governed by the presence of narrow micropores rather than total surface area, highlighting that the key performance factor was pore size matching to the kinetic diameter of CO_2 as. KOH provided the highest activation efficiency, while alternative potassium salts enabled milder pore development with improved yield. Oxygen-containing surface groups formed as a result of the activation contributed to adsorption energetics but remained secondary to textural effects under physisorption-controlled conditions.

Biomass- and recovered carbon black–derived carbons showed stable cyclic operation and favorable CO_2/N_2 selectivity under dilute and flue-gas-relevant conditions.

Beyond adsorption performance, this work demonstrates scalable routes for converting renewable, industrial, and technological carbon residues into high-value porous materials. The results provide design guidelines for precursor selection, activation strategy, and pore engineering in waste-derived carbons for gas separation and related environmental applications.

Keywords: Activated carbon; Waste valorization; Potassium activation; Recovered carbon black; Recovered graphite; Biomass; CO_2 capture; CCU, CCUS.

Acknowledgments

First and foremost, I would like to express my deepest gratitude to my supervisors, Professor Pavleta Knutsson and Professor Klas Andersson at Chalmers University of Technology, as well as Professor Renata Krzyżyńska at Wrocław University of Science and Technology. Their guidance, encouragement, and invaluable expertise have been instrumental throughout my research journey. Their continuous support, insightful advice, and confidence in my abilities have significantly contributed to both the completion of this work and my development as a researcher.

I would also like to extend my sincere appreciation to my colleague and friend, Jarosław Serafin. The many scientific discussions we shared have broadened my perspective, deepened my understanding of the field, and strengthened my enthusiasm for research. His friendship and intellectual support have been greatly valued.

My thanks go to all members of the Unit of Inorganic Environmental Chemistry and the Division of Energy Technology for fostering a collaborative, welcoming, and inspiring research environment. Their support and willingness to share knowledge have made my time in academia both productive and enjoyable.

I am also grateful to my friends at Chalmers, especially Joanna, Elena, Pedram, Kanming, and Hooman, for their friendship, encouragement, and the many memorable moments we shared throughout these years.

A special note of gratitude goes to my friend Maciej and Jason, whose unwavering friendship and support have been a constant source of strength and motivation..

Finally, I would like to thank everyone who has contributed, directly or indirectly, to my academic and personal growth. Your support, encouragement, and belief in me have played an important role in making this achievement possible.

Bartosz Dziejarski, Gothenburg (2026)

List of publications

This thesis is based on the following appended papers, which are referred to in the text by their assigned Roman numerals:

Paper I

Dziejarski, B*., Serafin, J., Hernández-Barreto, D. F., Naumovska, E., Sreńscek-Nazzal, J., Klomkliang, N., Tam, E., Krzyżyńska, R., Andersson, K., & Knutsson, P. (2025). Tailoring highly surface and microporous activated carbons (ACs) from biomass via KOH, $K_2C_2O_4$ and KOH/$K_2C_2O_4$ activation for efficient CO_2 capture and CO_2/N_2 selectivity: characterization, experimental and molecular simulation insights. ***Chemical Engineering Journal***, 169677.

Paper II

Dziejarski, B*., Hernández-Barreto, D. F., Moreno-Piraján, J. C., Giraldo, L., Serafin, J., Knutsson, P., Andersson K., & Krzyżyńska, R. (2024). Upgrading recovered carbon black (rCB) from industrial-scale end-of-life tires (ELTs) pyrolysis to activated carbons: Material characterization and CO_2 capture abilities, ***Environmental Research****, 247, 118169.*

Paper III

Dziejarski, B*., Faust, R., Serafin, J., Krzyżyńska, R., Andersson, K., & Knutsson, P. (2024). Insights into activation pathways of recovered carbon black (rCB) from end-of-life tires (ELTs) by potassium-containing agents, ***ACS Omega****, 9(29), 31814-31831.*

Paper IV

Dziejarski, B*., Fester, J. E. A., Serafin, J., Petranikova, M., Tam, E., Martinelli, A., Krzyżyńska, R., Andersson, K., & Knutsson, P. (2025). Valorization of hazardous graphite from black mass (NMC 111) of lithium-ion battery recycling via KOH activation for functional carbon design. ***Materials & Design****, 254, 114073.*

Related peer-reviewed papers not included in the thesis

Dziejarski, B*., Serafin, J., Andersson, K., & Krzyżyńska, R. CO_2 capture materials: a review of current trends and future challenges (2023), ***Materials Today Sustainability****, 24, 100483.*

Dziejarski, B*., Krzyżyńska, R., & Andersson, K. Current status of carbon capture, utilization, and storage technologies in the global economy: A survey of technical assessment (2023), ***Fuel****, 342, 127776.*

Serafin, J., & **Dziejarski, B.** (2024). Activated carbons—preparation, characterization and their application in CO_2 capture: a review. ***Environmental Science and Pollution Research***, 31(28), 40008-40062.

Serafin, J., & **Dziejarski, B**. (2023). Application of isotherms models and error functions in activated carbon CO_2 sorption processes. ***Microporous and Mesoporous Materials***, 354, 112513.

Serafin, J., **Dziejarski, B**., Junior, O. F. C., & Sreńscek-Nazzal, J. (2023). Design of highly microporous activated carbons based on walnut shell biomass for H_2 and CO_2 storage. ***Carbon***, 201, 633-647.

Fonseca-Bermúdez, Ó. J., Giraldo, L., Sierra-Ramírez, R., Serafin, J., **Dziejarski, B**., Bonillo, M. G., ... & Moreno-Piraján, J. C. (2024). Cashew nut shell biomass: a source for high-performance CO_2/CH_4 adsorption in activated carbon. ***Journal of CO_2 Utilization***, 83, 102799.

Serafin, J., **Dziejarski, B**., Vendrell, X., Kiełbasa, K., & Michalkiewicz, B. (2023). Biomass waste fern leaves as a material for a sustainable method of activated carbon production for CO_2 capture. ***Biomass and Bioenergy***, 175, 106880.

Serafin, J., **Dziejarski, B**., Fonseca-Bermúdez, Ó. J., Giraldo, L., Sierra-Ramirez, R., Bonillo, M. G., ... & Moreno-Piraján, J. C. (2024). Bioorganic activated carbon from cashew nut shells for H2 adsorption and H_2/CO_2, H_2/CH_4, CO_2/CH_4, $H_2/CO_2/CH_4$ selectivity in industrial applications. ***International Journal of Hydrogen Energy***, 86, 662-676.

Serafin, J., **Dziejarski, B**., & Sreńscek-Nazzal, J. (2023). An innovative and environmentally friendly bioorganic synthesis of activated carbon based on olive stones and its potential application for CO_2 capture. ***Sustainable Materials and Technologies***, 38, e00717.

Serafin, J., Vikram, S., **Dziejarski, B**., & Sahoo, S. (2023). An environmentally friendly synthesis method of activated carbons based on subabul (Leucaena leucocephala) sawdust waste for CO_2 adsorption. ***Journal of Cleaner Production***, 412, 137406.

Serafin, J., **Dziejarski, B**., Rodríguez-Estupiñán, P., Fernández, V. B., Giraldo, L., Sreńscek-Nazzal, J., ... & Moreno-Piraján, J. C. (2024). Effective synthesis route of renewable activated biocarbons adsorbent for high CO_2, CH_4, H_2, N_2, C_2H_4 gas storage and CO_2/N_2, CO_2/CH_4, CO_2/H_2, C_2H_4/CH_4 selectivity. ***Fuel***, 374, 132462.

* *Corresponding author*

Contribution report

Paper I Principal author with main responsibility for all the experimental work, conceptualization, methodology, validation, data curation, formal analysis, visualization, project administration, and writing.

Paper II Principal author with main responsibility for all the experimental work, conceptualization, methodology, validation, data curation, formal analysis, modeling, visualization, project administration, and writing.

Paper III Principal author with main responsibility for most of the experimental work, conceptualization, methodology, validation, data curation, formal analysis, visualization, project administration, and writing.

Paper IV Principal author with main responsibility for most of the experimental work, conceptualization, methodology, validation, data curation, formal analysis, modeling, visualization, project administration, and writing.

Table of Contents

Nomenclatures

List of abbreviations

AC	Activated carbon
ACs	Activated carbons
BET	Brunauer–Emmett–Teller
BM	Black mass
CBp	Pyrolytic carbon black
CCUS	Carbon capture, utilization, and storage
CH_3COOK	Potassium acetate
CLC	Chemical looping combustion
CO_2	Carbon dioxide
CO_2/N_2	Carbon dioxide/nitrogen selectivity
COFs	Covalent organic frameworks
DAC	Direct air capture
DFT	Density functional theory
EDS	Energy-dispersive X-ray spectroscopy
ELTs	End-of-life tires
EV	Electric vehicle
FT-IR	Fourier-transform infrared spectroscopy
GHG	Greenhouse gas
IAST	Ideal adsorbed solution theory
IPCC	Intergovernmental Panel on Climate Change
K_2CO_3	Potassium carbonate
$K_2C_2O_4$	Potassium oxalate
KCl	Potassium chloride
KOH	Potassium hydroxide
LiBs	Lithium-ion batteries
LFP	Lithium iron phosphate
LMO	Lithium manganese oxide
MOFs	Metal–organic frameworks

MSW	Municipal solid waste
N_2	Nitrogen
NCA	Lithium nickel cobalt aluminum oxide
NMC	Lithium nickel manganese cobalt oxide
PSD	Pore size distribution
PVDF	Polyvinylidene fluoride
rCB	Recovered carbon black
SEM	Scanning electron microscopy
SEM–EDS	Scanning electron microscopy with energy-dispersive X-ray spectroscopy
TCD	Thermal conductivity detector
TGA	Thermogravimetric analysis
vCB	Virgin carbon black
V_{MIC}	Micropore volume
V_{TOT}	Total pore volume
XPS	X-ray photoelectron spectroscopy
XRD	X-ray diffraction

List of symbols

C	Carbon content (wt.%)
H	Hydrogen content (wt.%)
I_D/I_G	Intensity ratio of D and G Raman bands (–)
N	Nitrogen content (wt.%)
O	Oxygen content (wt.%)
P	Pressure (bar)
P_0	Saturation pressure (bar)
P/P_0	Relative pressure (–)
R^2	Coefficient of determination (–)
S	Sulfur content (wt.%)
S_{BET}	Specific surface area ($m^2\ g^{-1}$)
V_{TOT}	Total pore volume ($cm^3\ g^{-1}$)

V_{MIC}	Micropore volume ($cm^3\ g^{-1}$)
$V_{MIC(N_2)}$	Micropore volume determined from N_2 adsorption at −196 °C ($cm^3\ g^{-1}$)
θ	Diffraction angle (°)

1. Introduction

1.1 The CO_2 challenge and the role of carbon capture, utilization, and storage (CCUS)

The accelerating increase in atmospheric carbon dioxide (CO_2) concentration remains one of the most critical environmental challenges of the twenty-first century. CO_2 is the predominant anthropogenic greenhouse gas, and its accumulation is the principal driver of global warming and climate instability [1]. In 2024, total energy-related CO_2 emissions increased by 0.8%, reaching an all-time high of 37.8 Gt CO_2. This rise contributed to record atmospheric CO_2 concentrations of 422.5 ppm, approximately 3 ppm higher than in 2023 and about 50% above pre-industrial levels. During the same year, CO_2 emissions from fuel combustion grew by around 1% (357 Mt CO_2), while those from industrial processes declined by 2.3% (62 Mt CO_2). Emissions growth remained below the global GDP increase of 3.2%, indicating a partial decoupling between economic expansion and emissions [2].

According to the Intergovernmental Panel on Climate Change (IPCC, 2022), immediate and coordinated mitigation actions are essential to limit global warming to 1.5 °C above pre-industrial levels. The IPCC projects that global greenhouse gas (GHG) emissions must peak by 2025 at the latest and decline by at least 43% by 2030 to achieve this target [3]. Meeting these ambitious goals requires a rapid transition to low-carbon technologies across all sectors, including power generation, transportation, and materials production, complemented by efficient, scalable, and sustainable methods for CO_2 capture and management.

Among the available strategies for CO_2 mitigation, carbon capture, utilization, and storage (CCUS) has emerged as a key enabling technology for deep decarbonization [4]. The schematic methodology for reducing both capturable and uncapturable CO_2 emissions through the CCUS framework is illustrated in **Figure 1**. In this system, CO_2 is primarily captured from major point sources such as power plants, cement and steel industries, and chemical manufacturing facilities, or directly from ambient air using Direct Air Capture (DAC) technologies. The captured CO_2 is then compressed and transported, typically via pipelines, ships, or trucks, to storage or utilization sites, where it can be permanently stored in geological formations such as depleted reservoirs and saline aquifers, or converted into valuable products including fuels, chemicals, and construction materials [5].

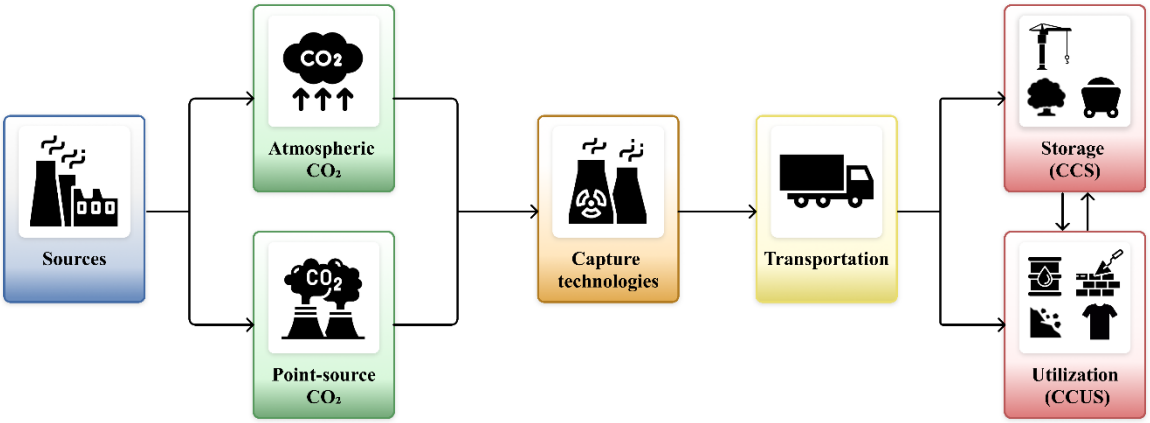

Figure 1. Schematic methodology for reducing CO_2 emissions through CCUS.

Carbon capture represents a critical limitation in CO_2 mitigation, as the separation step strongly influences both energy demand and overall process viability. In CCUS systems, CO_2 can be captured via pre-combustion, post-combustion, or oxy-fuel combustion configurations. To enable separation within these approaches, several technologies have been developed, including absorption (e.g., conventional amine scrubbing), adsorption, membrane separation, cryogenic methods, chemical looping combustion (CLC), and calcium looping (CaL). Within these approaches, adsorption-based CO_2 capture has gained increasing attention as an energy-efficient and environmentally sustainable alternative to amine-based absorption [6]. Adsorption processes operate under moderate conditions and allow repeated CO_2 uptake and release with low regeneration energy. In practical applications, this approach relies mainly on solid sorbents, valued for their high thermal stability, chemical robustness, and adjustable surface characteristics. Among the various materials investigated for gas sorption applications, including metal–organic frameworks (MOFs), covalent organic frameworks (COFs), zeolites, amine-functionalized solids, and carbon-based sorbents, considerable attention has been devoted to materials offering low cost, wide availability, low density, and well-developed porosity. These attributes support their use under diverse conditions. Activated carbons form a major and technologically mature subgroup within carbon-based sorbents and remain widely explored in CO_2 capture research [7].

1.2 Activated carbons development from waste-derived carbon resources

Activated carbon, one of the most extensively studied carbon-based adsorbents, play a crucial role in addressing environmental challenges. In their production, carbon-rich materials are used as precursors, which undergo physical or chemical activation to develop the desired porosity and surface characteristics. Ideally, suitable precursors are expected to possess high

carbon content, low ash levels, minimal volatile matter, and limited thermal degradation to maintain the desired physicochemical properties [8]. Traditionally, materials such as brown, bituminous, and anthracite coals, and peat have been employed in large-scale AC production due to their abundance, high carbon yield, and well-established processing technologies [9]. However, these conventional raw materials are finite, and not all are renewable, which has driven increasing research interest toward sustainable alternatives. With the growing emphasis on sustainability, attention has shifted toward renewable and waste-derived precursors with biological origin, such as agricultural residues, municipal wastes, animal by-products, forestry residues, and food industry wastes (**Figure 2**). These feedstocks, rich in lignocellulosic components (cellulose, hemicellulose, and lignin), offer significant potential for conversion into ACs with well-developed porous structures and large surface areas after carbonization and activation [10, 11].

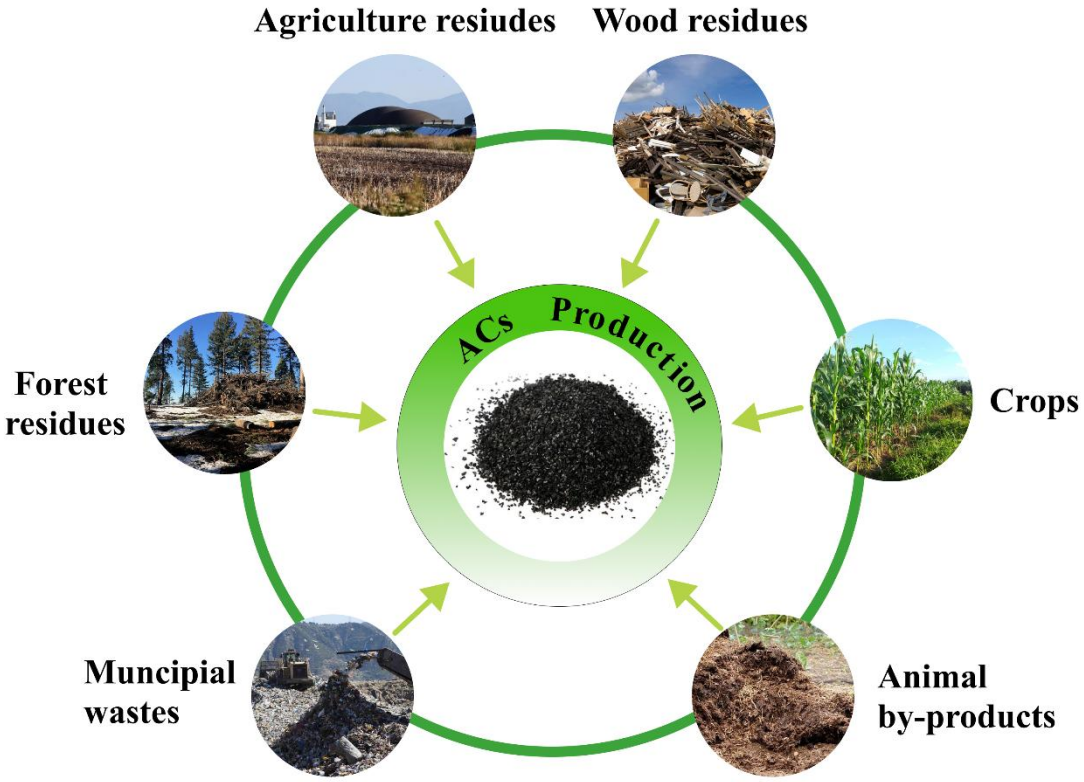

Figure 2. Available and suitable materials for the production of activated carbons.

Beyond biological products, with time and increasing demand for renewable technologies, it has become equally important to consider carbon-rich waste streams originating from industrial processes, which remain largely underutilized despite their high recovery potential. End-of-life tires (ELTs), for instance, represent a persistent environmental concern, continuously generated as by-products of the transportation sector [12]. In contrast, lithium-ion batteries (LiBs) are linked to emerging waste flows that are expected to grow considerably as

their use expands in sustainable energy systems [13]. Although battery wastes large-scale disposal is not yet critical, future projections indicate a substantial increase in waste volumes in the coming decades. Both recovered carbon black (rCB) obtained from ELT pyrolysis and graphite recovered from the black mass of spent batteries exhibit high carbon intensity, making them attractive precursors for the synthesis of functional porous materials. Even though available as streams and presenting potential for AC production, the industrial residue materials present complex composition and presence of inorganic and metallic impurities, which pose additional production challenges that require advanced processing and purification strategies [14, 15]. Integrating these industrial waste streams with biomass-derived precursors supports a comprehensive approach to waste valorization, enabling the transformation of diverse carbon sources into high-performance materials. In addition to the potential for CO_2 capture, the utilization of such feedstocks reinforces circular economy principles by minimizing environmental impact, enhancing resource efficiency, and contributing to carbon neutrality goals. A comparative overview of major carbon-rich feedstocks discussed in this thesis, including their global availability, distribution, future outlook, and associated challenges, is presented in **Table 1**.

Table 1. Comparison of major carbon-rich feedstocks, including their global availability, distribution, future outlook, challenges.

Stock	Availability	Geographical occurrence	Future outlook	Key challenges	References
Biomass residues	~3–5 Gt/year globally	Widespread but uneven; high in Asia, Europe, and USA	Rising demand toward 2050	Stock variability (moisture, ash) and seasonal availability	[16]
End-of-life tires	~1.5 Mt/year	Clustered in China, USA, EU with big vehicle fleets	Expected growth with transport sector expansion	Stock variability and processing challenges due to steel, ZnO, and additives	[17]
Lithium-ion batteries	~1.6-2 Mt/yr by 2030	Present in China, EU and USA (70% recycling in China; 10% EU/USA each.)	Strong rise post-2030 with EV market growth	Processing challenges arising from persistent metal impurities	[18]

2. Thesis overview

2.1 Aim and scope

The overall aim of this thesis is to develop routes for the synthesis of functional carbon materials from waste-derived precursors and to evaluate their potential for gas sorption applications, with particular emphasis on CO_2 capture (**Figure 3**). The work addresses the increasing need for circular and resource-efficient approaches to carbon material production by utilizing waste streams of biological, industrial, and technological origin. These include woody biomass, rCB from end-of-life tires, and graphite recovered from the black mass of spent LiBs. The focus is placed on establishing a mechanistic understanding of activation and conversion processes, optimizing synthesis parameters, and linking structural evolution to sorption performance.

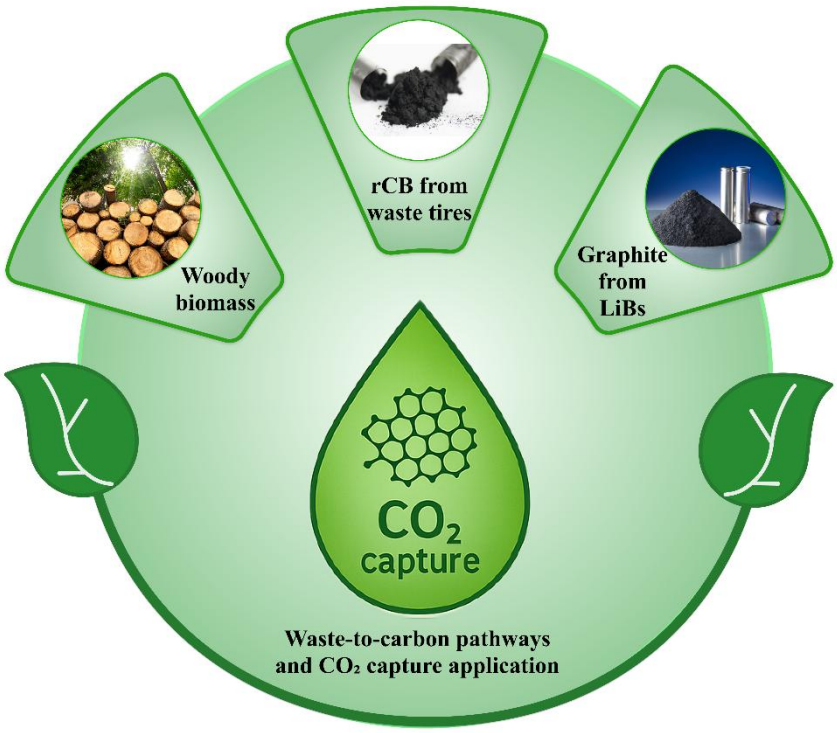

Figure 3. Illustration of the materials and the end-goal application within the framework of the current thesis.

More specifically, the research has been conducted to meet the following objectives:

- Follow the activation mechanisms of waste-derived precursors under potassium-based activation (KOH, K_2CO_3, CH_3COOK, $K_2C_2O_4$, KCl) and their impact on pore development and surface chemistry.

- Link structure and performance by combining textural, structural, and surface analyses to track how activation conditions shape micro- and mesoporosity and functional groups.
- Compare biomass, recovered carbon black, and recovered graphite to determine how precursor origin governs transformations, advantages, and limitations.
- Quantify CO_2 capture, emphasizing adsorption capacity, CO_2/N_2 selectivity, and cyclic stability.
- Outline scalable routes that convert waste carbons into high-value sorbents to advance circular economy goals and industrial decarbonization.

2.2 Outline

This thesis comprises the main findings from four appended papers (**Papers I-IV**) that investigate the activation of biomass- and waste-derived precursors into porous carbon materials for potential CO_2 capture applications. The work combines experimental studies to understand how the type of precursor, the type of potassium-based activator, and processing conditions affect pore development, surface chemistry, and structural properties of the obtained carbons. The development of the research work and its relation to the research papers are schematized in **Figure 4**.

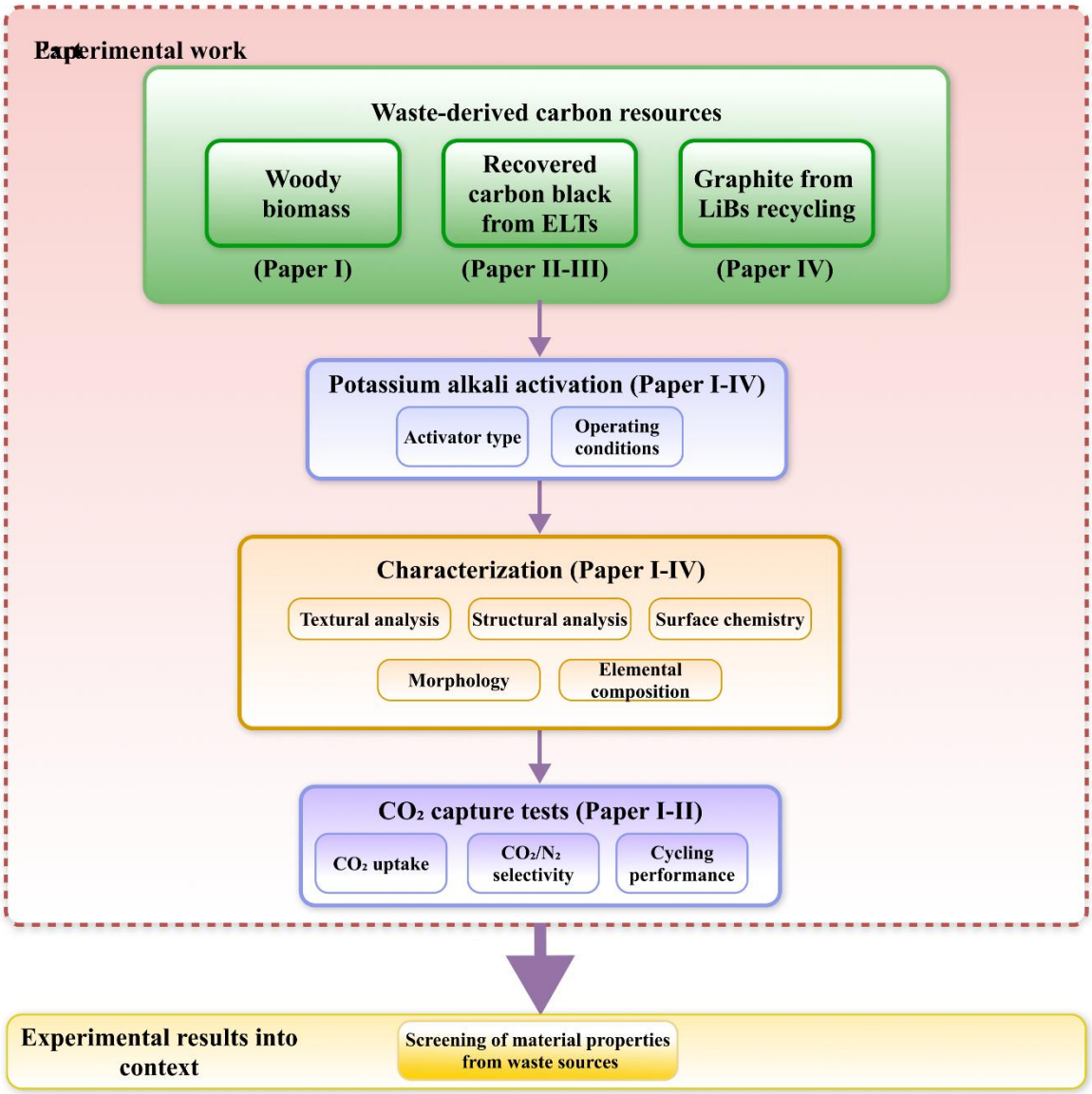

Figure 4. Overview of the research pathways and their connections to the papers included in this thesis.

Paper I focuses on the preparation of activated carbons from woody biomass using KOH, $K_2C_2O_4$, and their mixture as activating agents. The study compares the influence of these activators on pore formation, surface features, and CO_2 adsorption behavior, emphasizing the potential of $K_2C_2O_4$ as a more environmentally friendly alternative to conventional KOH activation. The work provides a foundation for understanding how activation conditions control the textural and CO_2 adsorption characteristics of highly surface and microporous biomass-derived carbons.

Paper II introduces the use of rCB from industrial-scale end-of-life tire pyrolysis as a carbon precursor. KOH was used as the activating agent to develop porous structures suitable for gas adsorption. The study includes characterization of the produced materials and evaluates their CO_2 capture performance in terms of adsorption capacity, selectivity, and cyclic stability. The work demonstrates the potential of rCB as a reliable and scalable raw material for activated carbon production and highlights its suitability for environmental applications.

Paper III continues the investigation of recovered carbon black by testing different potassium salts, such as KCl, K_2CO_3, CH_3COOK, and $K_2C_2O_4$, as activating agents. The work compares the effectiveness of the different salts and examines how temperature, activation time, and activator ratio affect the development of porosity and surface properties. The study helps identify the most suitable conditions and activators for improving the quality of carbon materials produced from industrial residues.

Paper IV extends the research to high-technology waste by converting graphite recovered from the black mass (NMC 111) of spent lithium-ion batteries into activated carbons using KOH. The study focuses on structural and surface changes during activation and demonstrates a sustainable route for transforming hazardous graphite waste into functional porous carbons with potential use in environmental and energy-related applications.

Together, the four papers present a consistent research path that connects the production of porous carbons from renewable, industrial, and technological waste sources. The thesis contributes to developing sustainable methods for converting carbon-rich residues into useful materials, supporting circular economy goals and potential CO_2 capture applications.

2.3 Scientific contribution

This thesis contributes to the development of sustainable ACs from biomass and industrial waste streams for potential CO_2 capture applications. The work also deepens the understanding of how potassium-based activation influences pore development, surface chemistry, and structure across different precursors. A unifying motivation behind the research is the close link between CO_2 emissions and the generation of carbon-rich byproducts in energy- and transport-intensive sectors. Both sectors are major CO_2 emitters and simultaneously produce substantial waste streams that require responsible management. Connecting these two challenges through the valorization of waste materials into functional adsorbents offers a pathway toward more sustainable industrial practices. Designing activation routes that are

energy efficient, rely on accessible salts, and can be broadly applied to diverse carbon-rich residues is therefore a crucial step in aligning CO_2 capture with circular economy principles.

The main contributions of this thesis are:

- Establishing activation strategies for biomass using KOH, $K_2C_2O_4$, and their mixture, highlighting the more environmentally friendly character of potassium oxalate.
- Extending KOH activation to rCB from end-of-life tires, including detailed characterization and CO_2 adsorption assessment.
- Comparing different potassium salts (KCl, K_2CO_3, CH_3COOK, and $K_2C_2O_4$) to determine their influence on porosity and surface properties of rCB.
- Demonstrating the valorization of graphite from lithium-ion battery black mass into functional porous carbons using KOH activation.
- Providing a unified understanding of potassium-assisted activation across renewable, industrial, and technological carbon sources.

Together, these studies demonstrate how coupling CO_2 capture with waste-stream valorization can support the transition toward circular economy principles and guide the development of more sustainable processes within carbon-intensive industrial sectors.

3. Theoretical background

3.1 Precursors for ACs production

The diversity of waste-derived precursors available for activated carbon production reflects the significant differences in chemical composition, structural characteristics, and practical processing constraints among the different precursors. To provide a structured comparison, **Table 2** summarizes representative feedstock categories explored in this thesis, highlighting their carbon content, compositional features, industrial handling limitations, and current recycling levels.

Table 2. Comparison of waste-derived feedstocks for activated carbon production.

Feedstock	Chemical and structural content	Restrictions for material use	Carbon intensity (C content, %)	Activated carbon production scale from this source
Biomass waste	Predominantly cellulose (35–50%), hemicellulose (20–35%), lignin (10–30%); minor ash, extractives, alkali and alkaline earth metals	Seasonal variability, heterogeneous composition, high moisture content, ash-related fouling, transport logistics, land-use competition	45–55% (dry basis)	Strong growth expected due to low-cost feedstock availability
End-of-life tires	Crosslinked elastomers, carbon black (30–35%), steel (~10–15%), additives (ZnO, sulfur, oils)	Hazardous classification, heavy metal residues, strict emissions regulations for pyrolysis, product quality standardization	70–85% (pyrolytic carbon black fraction)	Expected increase with rCB upgrading technologies
Lithium-ion batteries	Graphite (12–21%), cathode oxides, Cu/Al residues, PVDF binder, electrolyte salts	Hazardous waste classification, fluorinated binders, metal contamination, purification complexity, safety regulations	Graphite fraction: 90–99% C (purified); black mass overall: 20–30% C	Mostly pilot and demonstration scale

3.1.1 Biomass waste - a growing constraint and a carbon feedstock opportunity

Biomass is abundant in terrestrial and aquatic ecosystems and is also produced as industrial waste. The World Bioenergy Association estimates global standing biomass resources at approximately 1.804 trillion tonnes [19]. Annual biomass generation fluctuates strongly across seasons and regions due to climate, land management, and the distribution of cropland and forest, particularly in Europe and North America, but overall has increased over the past 22 years [20]. In 2022, EU biomass supply totaled ~1.2 billion tons of dry matter (tdm), dominated by primary biomass (directly harvested plant matter and residues) at 82%, followed by secondary biomass (processing by-products) at 7% and recovered or tertiary biomass (post-consumer waste streams) at 11% [21]. Within the primary fraction, agricultural crops, residues, and grazed biomass represented 67%, wood 33%, and fisheries and aquaculture <0.3% (dry matter). Beyond these primary inputs, additional residual streams arise from agro-industrial processing, livestock and industrial activities, sewage treatment, and municipal solid waste (MSW), which generate additional recoverable biomass residues. The recovery and use of biomass waste can partly displace fossil-based inputs, support rural development, and alleviate resource constraints. This recovery, however, is often limited by geographic dispersion, feedstock heterogeneity, and seasonal availability, which collectively increase the cost and emissions connected to collection, storage, and transport requirements and frequently result in material underutilization. On a global scale, wood-based biomass wastes are generated at ~4.6 Gt per year, with ~20% attributed to losses during production and processing, underscoring both the magnitude of the stream and the inefficiencies embedded in current value chains (**Figure 5**) [22].

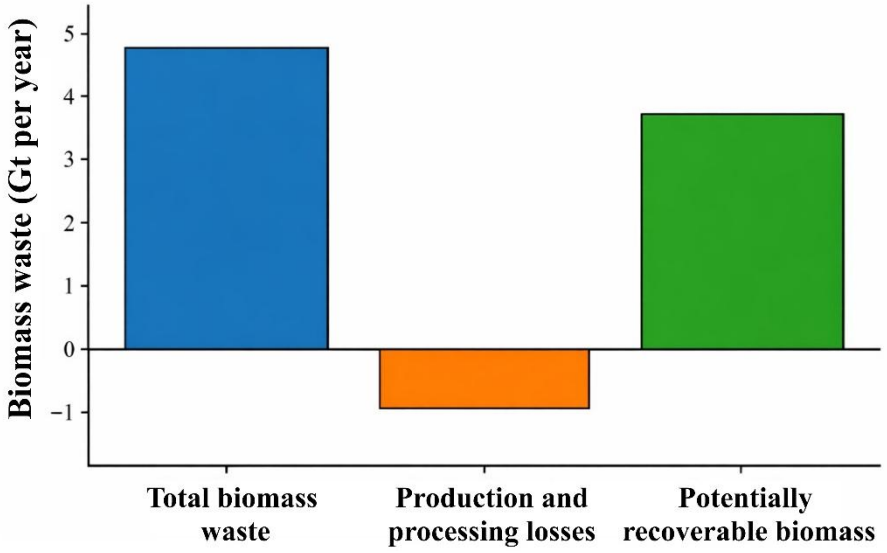

Figure 5. Mass balance of global wood biomass waste: total generation, losses, and potentially recoverable fraction.

The use of biomass-derived carbons and char-containing materials is gaining momentum across industries, as environmental compliance and sustainability targets increasingly prioritize lower emissions and cleaner production. Since wood represents a substantial fraction of primary biomass resources, forestry operations inherently generate large quantities of residual materials, including branches, treetops, bark, and low-grade roundwood [23], which are well suited for thermochemical conversion processes such as combustion, gasification, pyrolysis, and hydrothermal treatment [24]. In parallel, industrial processing produces significant volumes of secondary biomass, including sawdust and process-derived bark, forming carbon-rich by-products suitable for valorization. These streams represent particularly relevant feedstocks for the production of biochar and activated carbon, offering a pathway to partially substitute fossil-derived carbon materials.

3.1.2 End-of-life waste tires - valorization as a secondary carbon source

It is estimated that over 1 billion tires are manufactured and discarded worldwide each year, accounting for approximately 2% of total global solid waste generation [25]. The rapidly increasing accumulation of ELTs represents a persistent management challenge due to their durability, complex composition, and resistance to natural degradation, necessitating resource-efficient recovery strategies aligned with circular economy objectives. Effective ELT management requires coordinated action across the tire value chain, including manufacturers, recyclers, and regulatory bodies, to enable scalable material valorization pathways [26]. The ELT management challenge is further intensified by the global shift toward electric vehicles (EVs), which, due to their higher torque and vehicle weight, experience accelerated tire wear. Consequently, EV adoption is expected to increase the total volume of ELTs generated annually. For instance, in the United States, approximately 315 million ELTs are generated each year, and this figure is projected to rise by 12% to around 352 million by 2030 due to the growing EV market [27].

Globally, the management of ELTs follows several established pathways, including recycling (40–50%), energy recovery (30–40%), reuse (10–20%), and landfilling (5–10%), with exact shares depending on local regulations, technological maturity, and economic conditions (5–10%) [28, 29]. Despite progress in recycling, significant regional disparities remain. Developed countries operate advanced recycling and recovery systems, whereas many emerging economies still depend on landfilling and open dumping due to limited infrastructure

and weak policy enforcement. These practices pose serious environmental and health risks, as tires are chemically stable and degrade extremely slowly (releasing hazardous constituents such as heavy metals, polycyclic aromatic hydrocarbons, and organic additives), leading to soil and groundwater contamination. Uncontrolled burning releases toxic gases such as carbon monoxide, dioxins, and furans [30], while large stockpiles increase fire hazards and create breeding sites for disease-carrying insects.

Among existing treatment methods, pyrolysis has emerged as one of the most promising options for sustainable ELT management. During pyrolysis tires are decomposed in an oxygen-deficient environment to produce three main products: liquid oil, gas, and a solid carbonaceous residue known as pyrolytic carbon black (CBp) [31]. The solid fraction accounts for approximately 35–40% of the total output and is a critical factor determining the overall economic viability of the process. To obtain higher-value carbon materials, the solid pyrolysis residue must undergo further purification and refinement, yielding recovered carbon black. This material possesses properties comparable to those of virgin carbon black (vCB), which is conventionally produced through the partial combustion of petroleum-derived hydrocarbons [32]. Since vCB production is energy-intensive and emits substantial amounts of CO_2, substituting it with rCB provides both environmental and economic benefits. ELTs therefore represent a valuable secondary carbon resource capable of reducing dependence on fossil-based raw materials and supporting low-carbon manufacturing.

The quality of rCB depends strongly on tire composition, process parameters, and post-treatment efficiency. CBp typically contains additivies (1-3%), inorganic impurities (10-15%) such as zinc oxide (ZnO), silica (SiO_2), and sulfur compounds (e.g., FeS, ZnS), which can limit its performance compared with vCB, as shown in **Figure 6**. Achieving consistent and high-purity rCB requires optimization of the entire process chain, encompassing feedstock selection, pyrolysis control, and purification techniques [33]. Supportive policy measures and market incentives are essential to encourage the large-scale utilization of rCB and to establish standards for its industrial application.

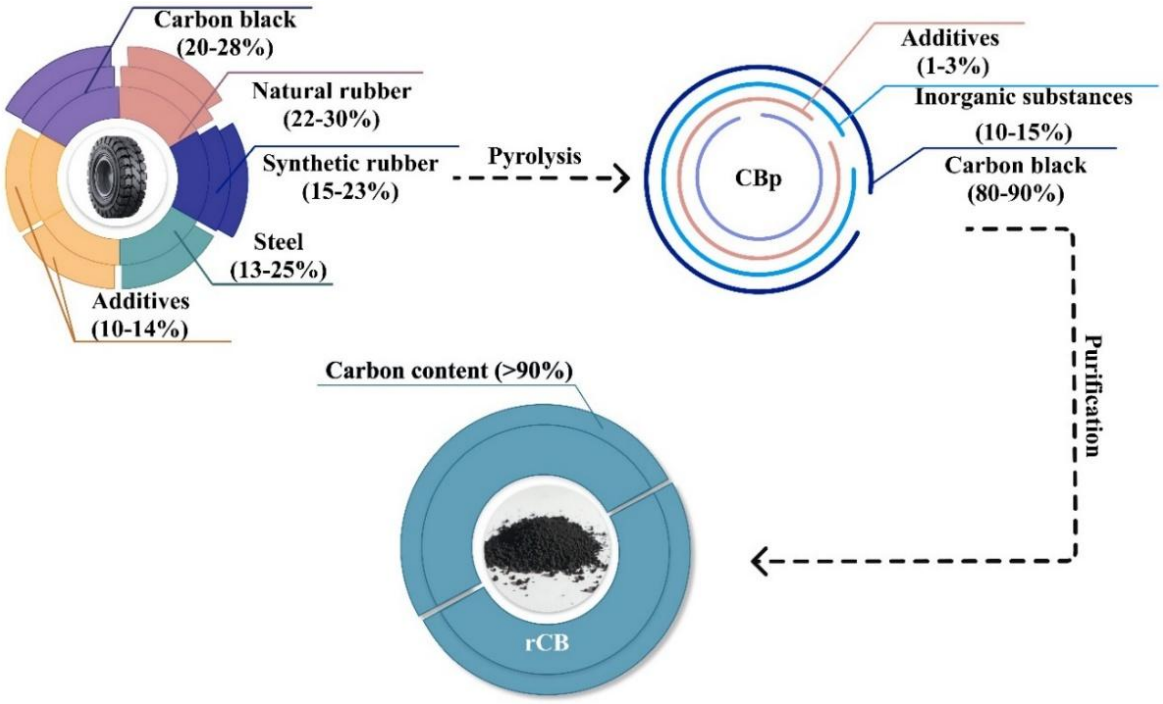

Figure 6. Schematic representation of the recycling pathway for end-of-life tires and the purification of pyrolytic carbon black into recovered carbon black, highlighting the transformation in material composition.

3.1.3 Lithium-ion batteries - graphite recovery and carbon feedstock utilization

The extensive integration of LiBs in electric vehicles and stationary storage systems has established them as a central technology in the transition toward sustainable, low-carbon energy systems. This expansion is reflected in global electric cars sales, which exceeded 17 million units in 2024, accounting for more than 20% of total car sales worldwide. This momentum continued into 2025, when global EV sales surpassed 20 million units, representing over one quarter of all vehicles sold globally and highlighting the accelerating electrification of the automotive sector [34]. Although only a limited number of EV batteries have reached end-of-life (EoL) so far, recycling facilities already process substantial quantities of production scrap, and forecasts suggest that more than 1.2 million EV batteries will be retired annually by 2030, increasing to over 14 million per year by 2040 [35]. In view of this, the heterogeneous architecture of LIBs, containing critical metals, reactive electrolytes, and polymeric components, complicates safe end-of-life handling and recycling, creating material recovery and environmental control challenges [36].

LiBs typically consist of metallic casings, cathode and anode materials, electrolytes, separators, and polymeric binders [37]. Among the broad range of cathode formulations used

in lithium-ion batteries, the dominant ones are lithium iron phosphate (LFP), lithium nickel manganese cobalt oxide (NMC), lithium nickel cobalt aluminum oxide (NCA), and spinel lithium manganese oxide (LMO) [38]. Among the enumerated cathode types, NMC ($LiNi_xMn_yCo_{1-x-y}O_2$) continues to dominate the automotive sector, largely due to their high specific energy, which typically reaches 100-265 Wh/kg [39]. Their development has progressed toward increasingly nickel-rich compositions, exemplified by the transition from NMC 111 to NMC 622 and NMC 811, where nickel content rises while manganese and particularly cobalt fractions are reduced [40].

In response to these material recovery challenges, the European Battery Regulation aims to close the material loop by enforcing ambitious recovery targets of up to 95% for Co, Ni, and Cu and 80% for Li by 2031 [41]. The current recovery process comprises pretreatment activities (sorting, discharging, disassembly, and crushing), pyrometallurgical steps such as smelting and roasting, and hydrometallurgical processes based on leaching and selective extraction [42]. The shredding or crushing of spent cells produces black mass (BM), a mixed fraction of cathode (Li, Ni, Mn, and Co) and anode materials, together with Cu and Al collectors, and polyvinylidene fluoride (PVDF) binders (**Figure 7**) [43]. Despite accounting for roughly 20% of the battery mass, the graphite anode receives considerably less attention [44].

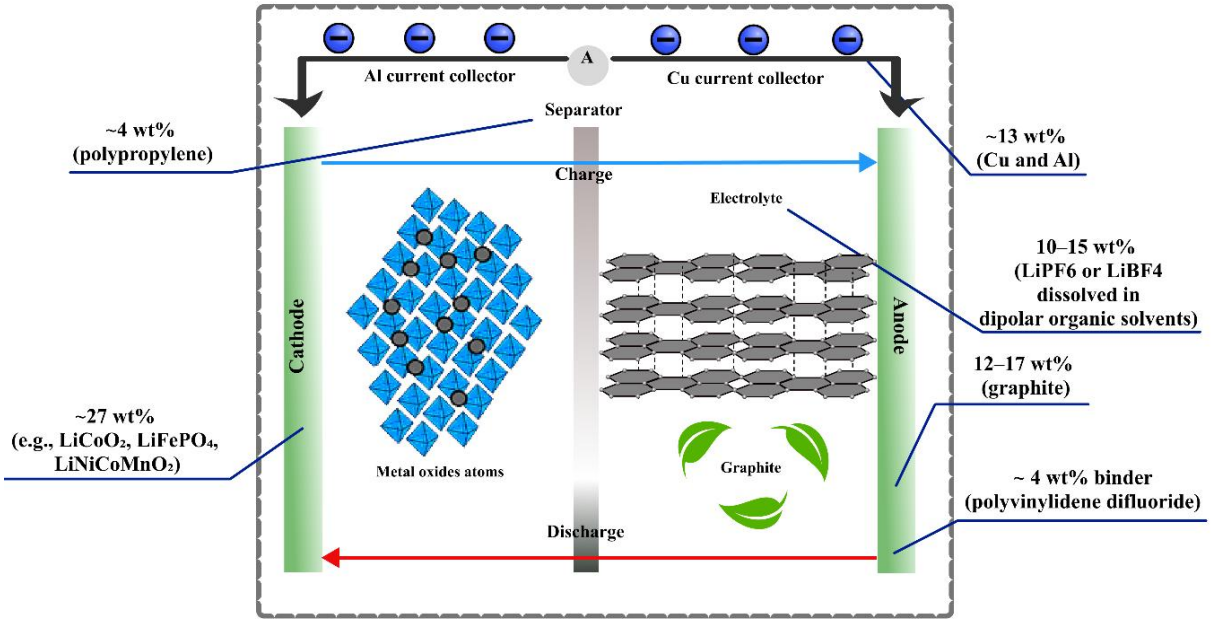

Figure 7. Structural overview of lithium-ion batteries in electric vehicles with specified material composition

Although graphite becomes the predominant component of black mass once metallic foils and polymers are removed, its recovery is often deprioritized due to the difficulty of

eliminating residual impurities left in the graphitic structure. Yet spent graphite remains a valuable and underutilized resource. Commercial anode graphite typically costs 8–13 USD kg^{-1}, accounting for 10–15% of the material cost in conventional LIBs, and spent batteries contain approximately 12–21 wt% graphite. These figures underscore the need for more comprehensive and resource-efficient recycling approaches [45]. The need for recovery is further amplified by projections from the World Bank, which estimate that by 2050 approximately 4.5 million tonnes of graphite will be required for low-carbon energy technologies, primarily LIBs, implying substantial growth in graphite consumption and corresponding waste generation [46]. Valorizing recovered graphite therefore represents a critical opportunity within a circular battery economy, as integrating its recovery into existing recycling infrastructure would reduce the environmental burden of black mass disposal while providing high-purity carbon precursors for advanced applications [47].

3.2 Activation of carbon materials

Carbon materials obtained after carbonization generally exhibit limited surface area and insufficient porosity for adsorption applications. Activation is therefore required to restructure the carbon framework and generate accessible pore networks [48]. Depending on the nature of the activating medium, activation is commonly classified into physical and chemical approaches, which differ significantly in their mechanisms, processing conditions, and degree of control over pore development.

3.2.1 Physical activation

Physical activation relies on the controlled gasification of carbon in the presence of oxidizing gases such as steam, CO_2, air or limited oxygen-containing mixtures. This process is typically conducted at high temperatures, generally in the range of 750–1000 °C, where porosity develops through gradual carbon burn-off [49]. Two principal routes can be distinguished, depending on whether activation is coupled with thermochemical conversion or conducted as a separate stage, corresponding to the direct and two-step strategies (**Figure 8**). While physical activation can effectively increase total porosity, the process is largely governed by reaction time and burn-off extent, which limits the possibility for precise control over pore size and distribution. Moreover, the high thermal demand and prolonged activation times associated with gas-phase routes impose substantial energy penalties, making physical activation less attractive for applications requiring finely tuned porosity.

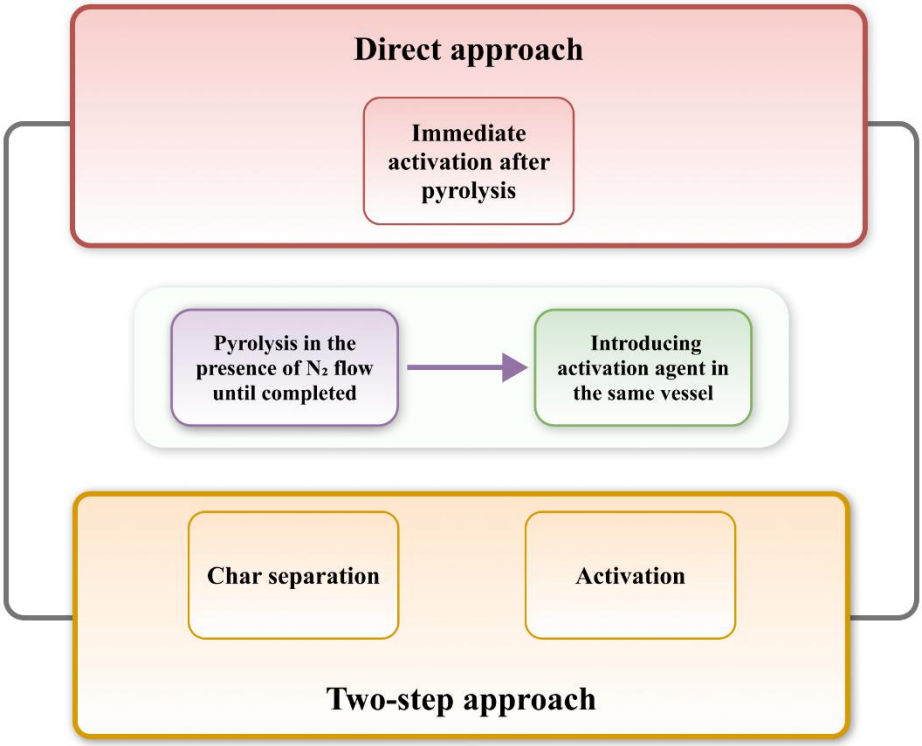

Figure 8. Schematic representation of the two physical activation routes distinguished by the mode of thermal conversion: direct and two-step approaches.

3.2.2 Chemical activation

Chemical activation is based on the interaction between a carbon precursor and a chemical agent, followed by heat treatment under an inert atmosphere. During this process, porosity develops through reactions whose nature depends on both the precursor and the activating agent. These include dehydration and cross-linking reactions, as well as redox driven carbon etching and lattice expansion, which collectively restructure the carbon framework. The extent and nature of pore development depend on several parameters, including precursor composition (C, H, O, N content), activation temperature (450–900 °C), residence time (1-4 h), heating rate (5-10 °C/min), impregnation conditions (dry mixing or wet impregnation), the precursor-to-activator ratio (1:1 to 1:6), and the activating agent employed (**Figure 9**). Compared with physical activation, chemical activation offers several advantages, including lower activation temperatures and shorter processing times, increased carbon yield, enhanced pore development, reduced energy and operational demands, and more effective generation of microporosity [50].

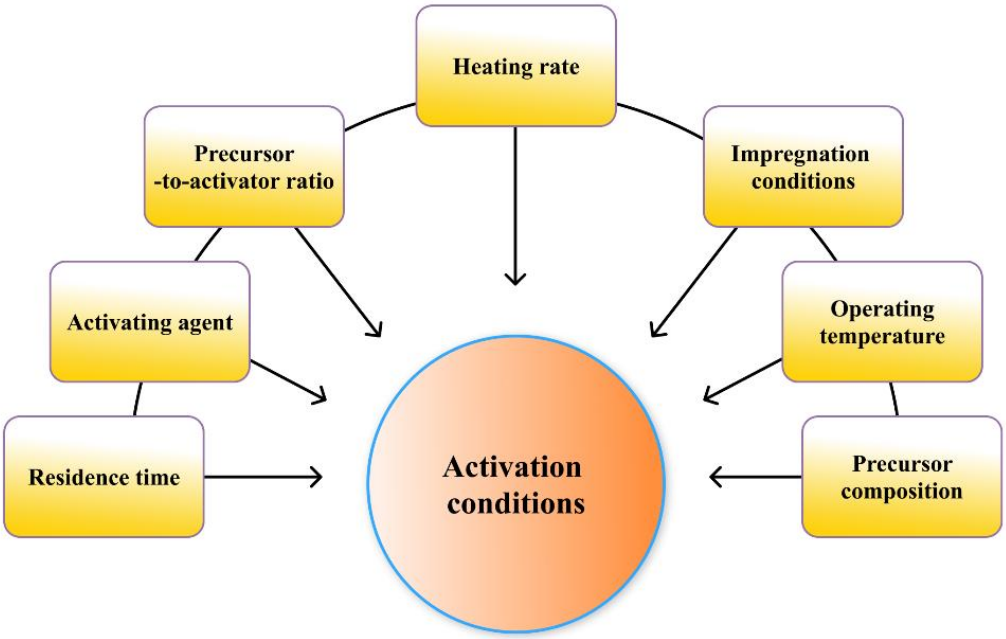

Figure 9. Key parameters in chemical activation affecting the properties of ACs.

Chemical activating agents are generally classified as alkaline agents (KOH, NaOH, K_2CO_3, Na_2CO_3, K_3PO_4), acidic agents (H_3PO_4, H_2SO_4, HNO_3), or Lewis-acid salts ($FeCl_3$, $ZnCl_2$,). These classes differ in their activation mechanisms and consequently in the pore structures they generate. Alkaline activators exhibit stronger chemical interaction with carbon matrices and are therefore more effective in producing microporous structures. In particular, KOH is considered to be highly efficient because it induces lattice expansion and carbon etching, as elemental potassium formed in situ intercalates into the carbon lattice and promotes structural expansion [51], but it can potentially cause excessive burn-off and reduced yield at high loadings [52]. This has led to increasing interest in alternative potassium salts, such as $KHCO_3$, K_2CO_3 and $K_2C_2O_4$, which typically operate at lower temperatures and provide improved yield retention and reduced environmental impact.

3.3 ACs applications

Activated carbons are versatile adsorbents widely used in water treatment to remove color, odor, taste, and diverse organic and inorganic contaminants, with additional applications in wastewater remediation (dyes [53-55], heavy metals [56-58], and phenolic compounds [59-61]), gas purification (CO_2 [62, 63], H_2S [64-66], SO_2 [67-69], NO_x [70-72], and volatile organic compounds [73-75]), and chemical, food, and pharmaceutical processing. Effective AC performance requires carefully tailored properties that satisfy application-specific technical and economic criteria. The key performance determinants can be grouped as follows [76, 77]:

- Adsorption capacity: determining the maximum uptake of target species.
- Selectivity toward specific adsorbates: enabling preferential removal in multicomponent systems.
- Pore characteristics, including pore size distribution and accessibility: mass transfer control and effective surface utilization.
- Surface chemical nature: influencing adsorbate–adsorbent interactions.
- Adsorption–desorption kinetics: governing uptake rates and process reversibility.
- Mechanical properties: ensuring resistance to attrition and structural degradation during operation.
- Chemical and thermal stability: allowing operation under aggressive chemical environments and elevated temperatures.
- Regenerability: reflecting the ability to restore adsorption performance after use.
- Stability over multiple adsorption–desorption cycles: indicating long-term durability.
- Production costs: affecting economic feasibility and large-scale deployment.

These requirements can be addressed through controlled material design, primarily by selecting appropriate activation strategies, including physical and chemical activation.

4. Experimental section

This research focuses on the production of high-performance activated carbons from diverse carbonaceous waste streams, including biomass, recovered carbon black from end-of-life tires, and graphite derived from lithium-ion battery recycling. Emphasis is placed on chemical activation strategies using potassium-based agents and their role in tailoring pore structure, surface chemistry, and adsorption behavior.

This section describes the complete experimental workflow, from raw material recovery and activation to comprehensive physicochemical characterization and adsorption performance evaluation. Each subsection provides a structured overview of the methodologies used to link material design with functional performance in gas separation. References to the corresponding publications are introduced within the relevant material-specific sections.

4.1 Materials

This thesis is based on three distinct carbonaceous waste streams: biomass, recovered carbon black from end-of-life tires, and graphite derived from lithium-ion battery recycling. **Figure 10** outlines the processing routes applied to the carbonaceous waste streams considered

in this thesis, illustrating their conversion into activated carbons for CO_2 capture. In this context, **Table 3** summarizes the main elemental composition of the examined waste streams. The values reported are normalized elemental contents, with the oxygen content calculated based on mass balance.

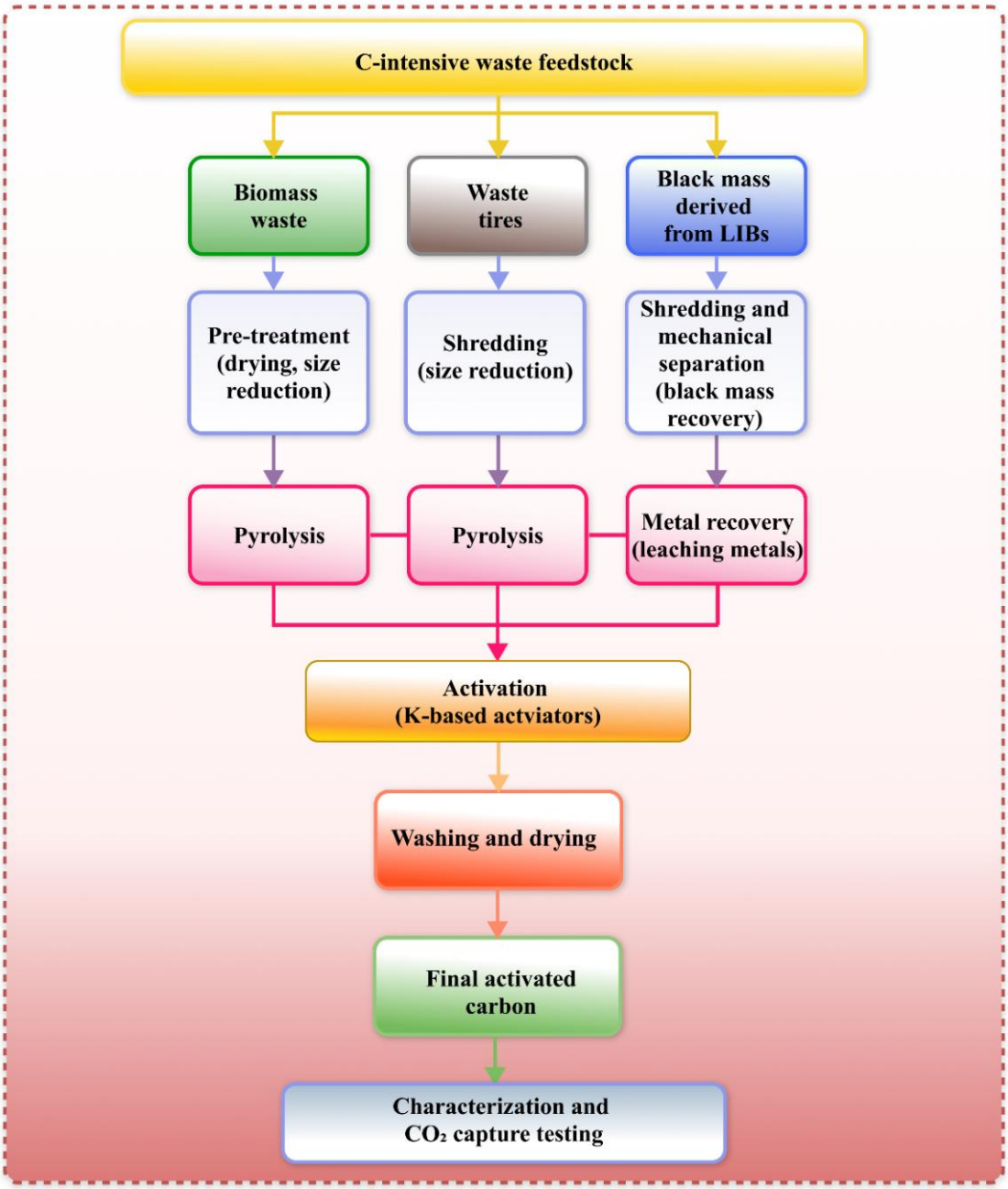

Figure 10. Integrated pathway for valorization of C-intensive waste feedstocks into activated carbons.

Table 3. Elemental composition of the carbonaceous waste streams considered in this thesis

Element	Composition (wt.%)		
	Woody biomass	Recovered carbon black	Recovered graphite
C	50.00	92.53	72.18
H	6.00	1.16	-
N	0.11	0.42	-
S	0.89	0.71	-
O	43.00	5.18	9.13

4.1.1 Woody biomass

Pine wood was used as the biomass precursor in Paper I and was obtained as residual wood fractions originating from conventionally harvested coniferous trees processed for energy applications. The material was collected during routine fuel handling at the plant facility of Chalmers University of Technology (Sweden), following standard forestry processing and mechanical pre-conditioning procedures, listed below and presented in **Figure 11**.

- **Forestry processing and wood preparation**

Following tree felling, the wood was sectioned and processed into fuel-grade pieces through standard forestry and wood-handling operations.

- **Mechanical pre-conditioning of biomass**

Pine wood was mechanically processed to reduce particle size and improve uniformity prior to activation. Milling produced a fine powder (<0.5 mm), facilitating consistent dry mixing and subsequent thermal treatment.

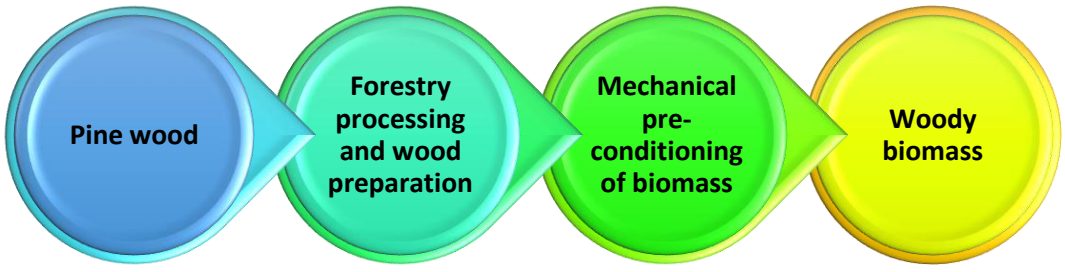

Figure 11. Schematic overview of the main steps involved in woody biomass pretreatment prior to activation.

It should be noted that the biomass had not been subjected to any chemical treatments, preservation processes, or surface modifications prior to use, ensuring that it remained a raw and unaltered lignocellulosic feedstock.

4.1.2 Recovered carbon black (rCB)

The recovered carbon black used in this work was derived from ELTs and served as the primary precursor material in **Paper II** and **Paper III**. The rCB was produced via industrial-scale pyrolysis of ELTs, followed by a sequence of post-treatment and purification steps designed to enhance its physicochemical quality, as illustrated in **Figure 12.** As a result of these processing steps, the obtained rCB exhibited an average particle size of approximately 30 μm, with particle sizes ranging from 15 to 100 μm and a dominant fraction between 73 and 80 μm.

- **Pyrolysis for pyrolytic char production**

Pyrolysis is the chosen thermochemical process in which ELTs were decomposed at temperatures exceeding 500 °C under an oxygen-free atmosphere. This inert environment prevented combustion and promoted the controlled breakdown of polymeric components, including natural and synthetic rubbers composed of long-chain macromolecules. The process yielded three main fractions: a solid carbonaceous char, a condensable liquid oil, and a non-condensable gaseous phase.

- **Post-pyrolysis processing**

Following pyrolysis, the resulting material contained various contaminants, including residual ash, organic residues, inorganic compounds, and partially reacted or unreacted hydrocarbons, as well as elements such as Zn, Si, Ca, S, and Al. Therefore, additional post-pyrolysis processing steps based on chemical or physical treatments were required to reduce these impurities. The removal of inorganic species enhanced the quality and applicability of the char by increasing the elemental carbon content and improving porosity.

- **Purification steps**

To convert pyrolytic char into commercially viable recovered carbon black, a series of purification and post-treatment steps was applied. These processes included concentrated pickling, devolatilization, milling and pulverization and, when required, pelleting, to further remove residual impurities, control particle size distribution, and reduce variability in material quality.

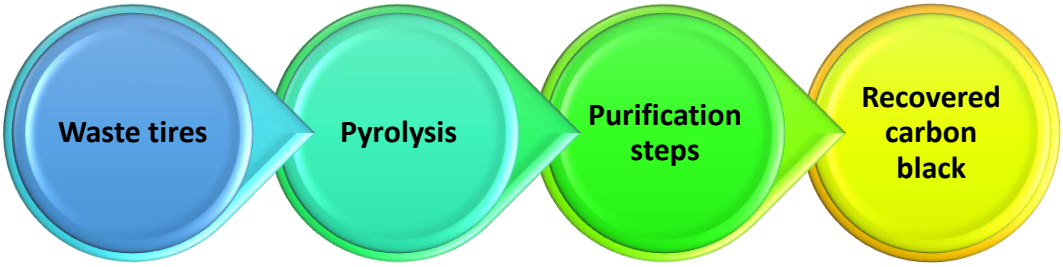

Figure 12. Overview of the general steps in rCB production from waste tires.

4.1.3 Graphite derived from LiBs recycling

The graphite used in this work was derived from end-of-life lithium-ion battery packs with NMC 111 chemistry and served as the primary precursor material in **Paper IV**. The material originated from industrial battery recycling streams and was obtained following battery discharge, disassembly, and mechanical processing carried out by industrial partners. A subsequent pre-treatment route was applied to upgrade the black mass and enable graphite recovery, as illustrated in **Figure 13**.

➢ **Industrial processing of lithium-ion batteries**

As part of the industrial recycling workflow, NMC 111 battery packs underwent controlled discharge, dismantling, and mechanical separation to isolate a fine particulate fraction known as black mass. This intermediate product represents a mixed stream containing electrode materials and served as the starting point for the subsequent graphite recovery and purification steps.

➢ **Post-processing of black mass**

The obtained black mass was further sieved to particle sizes below 500 µm to improve homogeneity and concentrate the carbonaceous fraction. After this treatment, the material remained a complex mixture of graphite, residual active materials, other inorganic species, and polymeric binders.

➢ **Purification and conditioning steps of black mass via acid leaching**

A purification and conditioning route based on acid leaching using H_2SO_4 in the presence of H_2O_2 was applied to reduce impurity content and enable the recovery of a graphite-rich precursor suitable for subsequent activation.

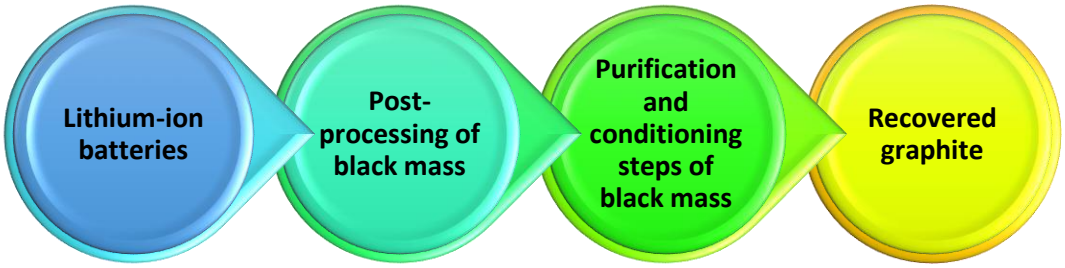

Figure 13. Process chain for graphite recovery from LiBs.

4.2 Analytical techniques

In this thesis, complementary analytical techniques were used. **Table 4** provides an overview of these techniques including their underlying principles, analytical outputs, and position within the characterization workflow.

Table 4. Summary of analytical techniques used in this thesis.

Technique	Theoretical basis	Information obtained	Role in workflow
Ultimate analysis	Combustion-based elemental quantification	C, H, N, S, O composition	Initial precursor and final material characterization
Proximate analysis	Thermogravimetric mass-loss analysis	Moisture, volatile matter, fixed carbon, ash	Thermal behavior and material classification
N_2 adsorption–desorption	Physisorption and multilayer adsorption	Surface area, pore volume, mesopore distribution	Post-activation structural evaluation
CO_2 adsorption	Micropore filling at controlled temperature	Micropore volume and pore size distribution	Detailed microporosity assessment
FT-IR spectroscopy	Infrared vibrational absorption	Surface functional groups	Chemical surface characterization
Raman spectroscopy	Inelastic photon scattering (Raman effect)	Structural order, defect density, graphitization	Carbon framework evaluation
SEM–EDS	Electron–matter interaction and X-ray emission	Morphology and elemental distribution	Microstructural and compositional analysis
XRD	X-ray diffraction from crystalline planes	Phase composition and crystallinity	Structural evolution assessment
XPS	Photoelectron emission from surface atoms	Surface elemental states and bonding	Surface chemistry evaluation

4.2.1 Ultimate and proximate analysis

Ultimate analysis is employed to determine the elemental composition of materials, typically quantifying carbon, hydrogen, nitrogen, sulfur, and oxygen calculated by difference [78]. The analysis is commonly based on the Dumas combustion principle, in which the sample undergoes rapid and complete oxidation through flash combustion. The resulting gaseous products are separated chromatographically and quantified using a thermal conductivity detector (TCD), generating signals proportional to the concentration of each element. Ultimate analysis provides fundamental insight into chemical composition.

Proximate analysis, in contrast, assesses the bulk physical composition by determining moisture content, volatile matter, fixed carbon, and ash. This analysis is frequently conducted using thermogravimetric methods, where mass changes are monitored as a function of temperature, allowing evaluation of thermal behavior and compositional fractions. Proximate analysis is particularly informative for assessing thermal stability, combustion behavior, and handling characteristics of carbonaceous materials.

In this thesis, ultimate and proximate analyses were applied in **Papers I–IV** to both precursor wastes and the resulting activated carbons. Together, these techniques provided complementary information on elemental composition and physical structure, supporting optimization of activated carbons.

4.2.2 N_2 and CO_2 adsorption-desorption isotherm analysis

Gas adsorption is a widely applied technique for characterizing the textural properties of porous materials, including specific surface area, pore volume, and pore size distribution (PSD). The method is based on controlled adsorption of a probe gas using dedicated instrumentation comprising a sample cell, precise pressure regulation, and gas dosing systems. Incremental amounts of adsorbate are introduced, and equilibrium uptake at each pressure step is used to define discrete points along the adsorption isotherm. During measurement, gas molecules physisorb onto the solid surface and interact with the pore walls through physisorption mechanisms that depend on pore size and adsorbate–adsorbent interactions at pressures below the saturation pressure (P_0) [79]. At low relative pressures (P/P_0), adsorption proceeds through micropore filling in microporous materials and monolayer formation on external and nonporous surfaces.. With increasing pressure, multilayer adsorption develops on open surfaces, while capillary condensation may occur in mesopores, producing a characteristic plateau in the isotherm [80]. Upon pressure reduction, desorption often follows a different path,

particularly in mesoporous materials, resulting in hysteresis due to delayed evaporation of condensed adsorbate. This hysteresis loop closes once condensed adsorbate is removed and equilibrium surface coverage is restored.

According to the IUPAC classification, six fundamental types of adsorption isotherms are distinguished, as presented in **Figure 14**. Type I isotherms describe adsorption in microporous materials and are characterized by rapid uptake at low pressures followed by saturation, consistent with the Langmuir model. Type II isotherms represent reversible multilayer adsorption on nonporous or macroporous solids, featuring a distinct inflection point that marks completion of monolayer coverage and the onset of multilayer adsorption. Type III isotherms arise from weak adsorbent–adsorbate interactions and show enhanced adsorption at higher relative pressures due to adsorbate–adsorbate interactions. Type IV and V isotherms are associated with mesoporous materials and exhibit hysteresis caused by capillary condensation; Type IV follows Brunauer–Emmett–Teller (BET) behavior at low pressures, while Type V reflects weaker surface interactions. Type VI isotherms, typical of uniform nonporous surfaces, display stepwise multilayer adsorption.

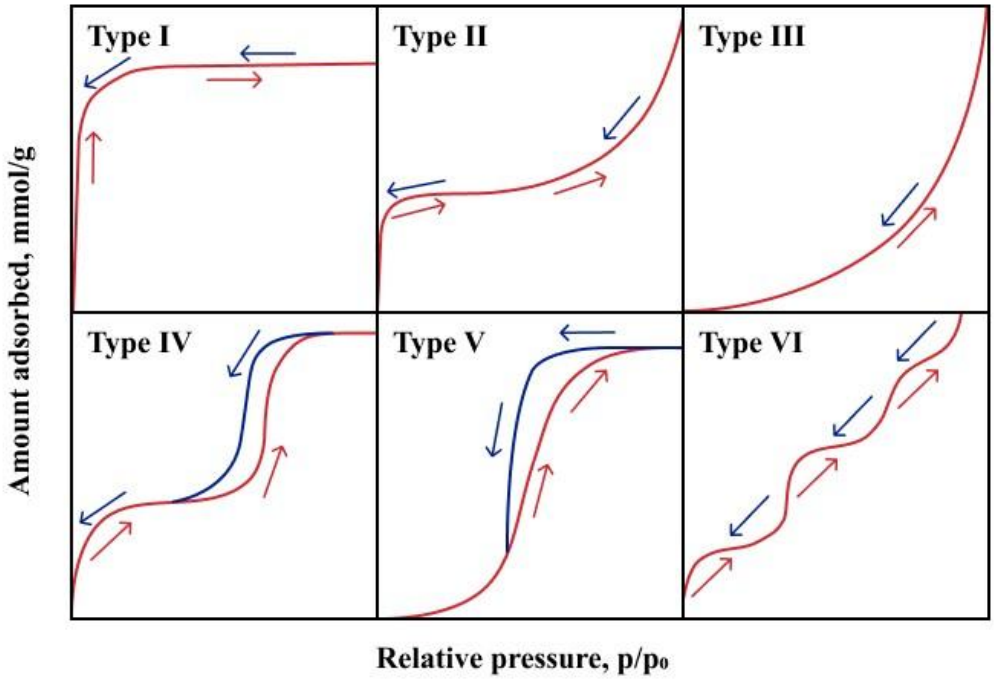

Figure 14. Classification of adsorption-desorption isotherms (red arrows: adsorption course; blue arrows: desorption course) [49].

Textural parameters are commonly derived from N_2 adsorption measurements at −196 °C. The total pore volume is estimated from the adsorbed N_2 quantity at a relative pressure close to saturation ($P/P_0 \approx 0.99$), where pores are commonly assumed to be filled by condensed

adsorbate[81]. The specific surface area is calculated using the BET equation, typically applied within the relative pressure range of 0.05–0.35, based on the formation of a complete monolayer followed by multilayer adsorption and selected according to established consistency criteria [82]. Since N_2 diffusion into ultramicropores may be kinetically limited at cryogenic temperatures due to kinetic restrictions arising from its molecular size(0.364 nm), quadrupole moment and low measurement temparature, CO_2 adsorption at 0 °C is frequently employed as a complementary technique to probe micropores below approximately 1 nm. Combined N_2 and CO_2 adsorption data enable PSD analysis across different pore size regimes, typically 2–50 nm for N_2 and 0.3–1.4 nm for CO_2. These distributions are calculated using density functional theory (DFT), which accounts for pore geometry and adsorption thermodynamics to provide a detailed description of pore structure and volume contributions [83].

In this thesis, N_2 adsorption–desorption measurements were systematically applied in **Papers I–IV** to determine BET surface area, total pore volume, mesopore volume, micropore volume (<2 nm), and PSD of activated carbons. Additionally, CO_2 adsorption experiments were performed in **Papers I** and **II** to further quantify micropore volume (0.3–1.4 nm) and refine PSD analysis.

4.2.3 Fourier-transform infrared spectroscopy (FT-IR)

Fourier-transform infrared spectroscopy (FT-IR) is a vibrational spectroscopic technique that combines infrared radiation with Fourier transformation to obtain high-resolution spectral information. The method enables identification of chemical functional groups in organic, polymeric, and selected inorganic materials through characteristic absorption features observed in FT-IR spectra. An FT-IR spectrometer operates based on an interferometer, which constitutes its central component. Infrared radiation is divided into two beams: one reflected by a fixed mirror and the other by a moving mirror. The recombination of these beams generates an interference pattern that varies with mirror displacement and is recorded as an interferogram. This interferogram contains contributions from all infrared frequencies interacting with the sample and is mathematically converted into an absorption spectrum through Fourier transformation [84].

For activated carbons, FT-IR spectroscopy is particularly valuable for examining surface functional groups, which significantly influence adsorption behavior toward organic compounds, contaminants, and gaseous species in both aqueous and gas-phase environments. The presence and nature of oxygen-containing and other surface functional groups provide insight into surface chemistry and potential adsorption mechanisms.

In this thesis, FT-IR spectroscopy was used to analyze the surface chemistry of activated carbons in **Papers I-II**.

4.2.4 Raman spectroscopy

Raman spectroscopy is a non-destructive analytical technique that provides information on molecular structure, chemical bonding, and lattice vibrations of materials. The technique is based on the Raman effect, which arises from the inelastic scattering of incident photons by molecular vibrations, leading to an energy shift relative to the excitation light [85]. While most photons undergo elastic (Rayleigh) scattering without energy change, a very small fraction experiences inelastic scattering, producing characteristic energy shifts that correspond to specific vibrational modes of the material.

A Raman spectrometer primarily consists of a monochromatic laser source, which illuminates the sample. The scattered light is collected, spectrally filtered using a monochromator, and detected by a charge-coupled device (CCD) detector [86]. The resulting Raman spectrum presents signal intensity as a function of Raman shift, typically expressed in wavenumbers (cm^{-1}), and serves as a molecular fingerprint of the analyzed material. Raman spectroscopy is particularly well suited for carbon-based materials, including activated carbons, graphene derivatives, carbon nanotubes, and related structures, due to its sensitivity to carbon bonding environments and structural disorder.

In this thesis, Raman spectroscopy was employed to evaluate the structural features of activated carbons. The technique provided insight into the degree of graphitization and defect density of the carbon framework, as discussed in **Paper II** and **Paper IV**.

4.2.5 Scanning electron microscopy (SEM) coupled with energy-dispersive X-ray spectroscopy (EDS) analysis

Scanning electron microscopy (SEM) is a powerful imaging technique used to examine surface morphology and microstructural features of materials. An SEM system comprises three main components: an electron gun, which generates and accelerates the electron beam; an electron column, where electromagnetic lenses and apertures shape and focus the beam; and a sample chamber, in which interactions between the electron beam and the specimen occur [87].

High-quality imaging requires focusing of the electron beam to achieve a small probe size while maintaining sufficient beam current. This is accomplished through a combination of condenser and objective lenses, which control beam convergence and focus it at the specimen surface. When the electron beam interacts with the sample, several signals are generated,

including secondary electrons (SE), backscattered electrons (BSE), and characteristic X-rays. These signals originate from different interaction volumes and provide complementary information.

In this thesis, SEM–EDS was employed in **Papers I–IV** to examine the morphological features of activated carbons and to identify elemental composition and spatial distribution after activation. Particular attention was given to evaluating the distribution of potassium following chemical activation.

4.2.6 X-ray diffraction (XRD) analysis

X-ray diffraction (XRD) is a widely used analytical technique for qualitative and quantitative assessment of material structure, providing information on crystalline phases and degree of crystallinity. The technique is based on the constructive interference of X-rays scattered elastically by periodic lattice planes within a crystalline material [88]. In a typical XRD setup, polychromatic X-rays generated in an X-ray tube (commonly using Cu or Mo radiation) are monochromatized and directed toward the sample. Interaction of the incident beam with crystal lattice planes produces diffraction when the Bragg condition is satisfied, resulting in a characteristic diffractogram.

In this thesis, XRD was applied in **Paper I, Paper III,** and **Paper IV** to identify changes in the relative contributions of amorphous and graphitic-like crystalline structures during chemical activation using potassium-based activating agents. The technique provided insight into the influence of potassium compounds on the structural evolution of ACs. XRD patterns were interpreted through qualitative comparison with reference data from the ICDD PDF-4+ 2025 database.

4.2.7 X-ray photoelectron spectroscopy (XPS) analysis

X-ray photoelectron spectroscopy (XPS), also known as electron spectroscopy for chemical analysis (ESCA), is a surface-sensitive technique used to determine elemental composition and chemical bonding states within the outermost surface (few nanometers) of a material. The method is based on the emission of core-level electrons induced by X-ray irradiation, with the kinetic energy of the emitted photoelectrons measured by an electron energy analyzer [89].

Because binding energies are characteristic of both the element and its chemical environment, XPS enables identification of surface elements and analysis of both their chemical bonding and oxidation states. Survey scans provide rapid elemental detection, while high-

resolution spectra yield detailed chemical state information. When combined with Ar^+ ion sputtering, XPS can also be used for depth profiling, making it a powerful tool for surface and interface analysis in materials science.

In this thesis, XPS was applied in **Paper I** and **Paper IV** to investigate surface elemental composition and chemical states of activated carbons, providing insight into the influence of activation conditions on surface chemistry and functional group evolution.

4.3 Methods

In this thesis, this section presents the methodologies used for the synthesis of ACs and for evaluating their CO_2 adsorption performance. The section is organized into two main subsections covering AC preparation and CO_2 adsorption studies, with detailed descriptions of the used experimental procedures, setups, and operating conditions.

4.3.1 Preparation of ACs

The conversion of the three investigated waste-derived precursors into activated carbons was performed via potassium-mediated chemical activation using a dry mixing approach. KOH was applied as the activating agent in all studies, as the most established activator in the literature (**Papers I–IV**). In addition, alternative potassium-based compounds, including K_2CO_3, KCl, CH_3COOK, and $K_2C_2O_4$, were investigated in **Paper III** as activating agents or reference additives to assess their impact on pore formation and structural evolution of rCB. **Paper I** further examined mixed activating systems based on combined KOH and $K_2C_2O_4$ formulations to identify potential synergistic effects during the chemical activation of biomass, with additional emphasis on improving the environmental friendliness of the activation process.

Prior to activation, the waste-derived precursors were subjected to appropriate conditioning and mechanical size reduction to obtain homogeneous powdered materials. The activation route involved solid–solid blending of the precursors with the selected potassium-containing reagents, carried out by manual grinding in a mortar to ensure uniform dispersion. The resulting mixtures were placed in alumina crucibles and thermally treated in a horizontal tubular furnace operated under a continuous N_2 flow to maintain inert conditions. A schematic representation of the preparation of the ACs workflow is provided in **Figure 15**.

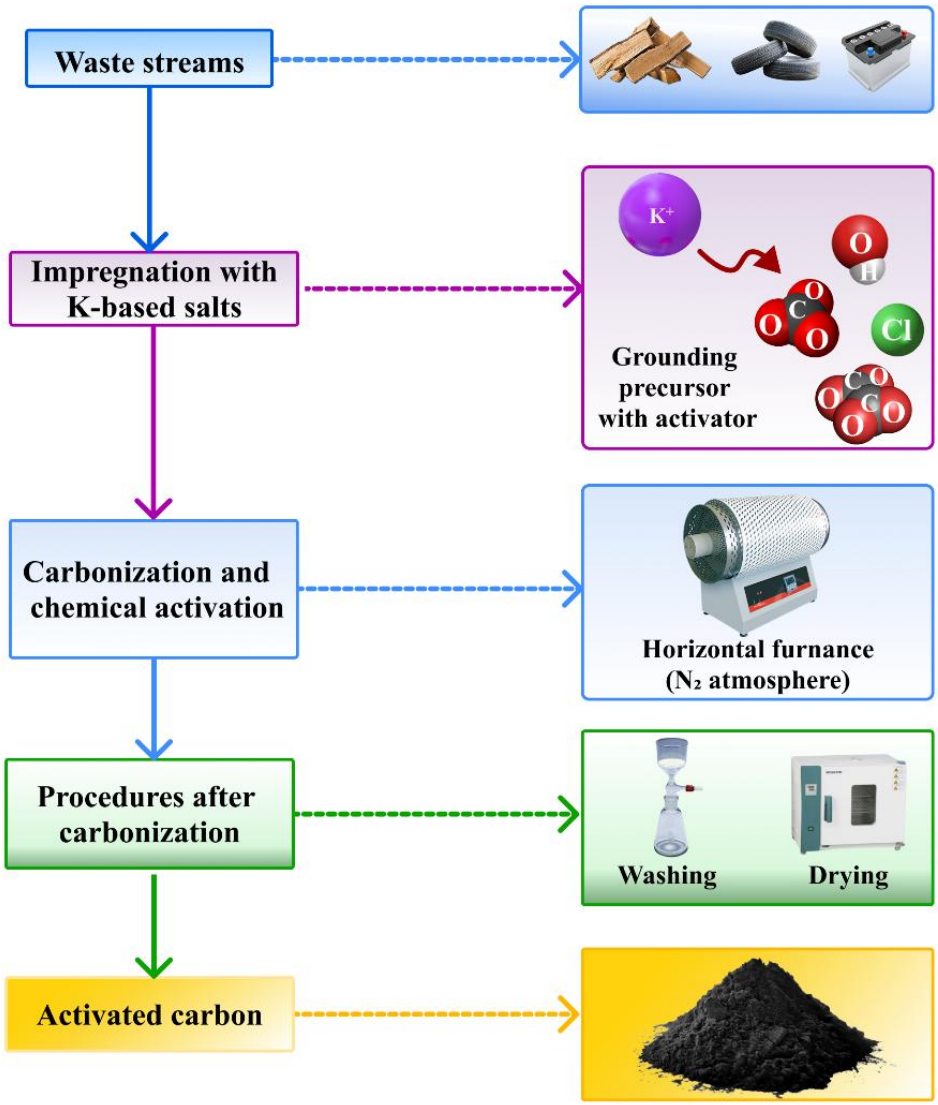

Figure 15. Schematic illustration of the different stages in the preparation of activated carbon from waste streams via K-based chemical activation.

Thermal activation was performed using parameters selected to promote effective carbonization and controlled development of porosity. The activation temperature profiles, residence times, heating rates, and precursor-to-activator mass ratios were established through systematic optimization based on preliminary experiments and literature reviews. Following thermal treatment, the activated materials were thoroughly washed with deionized water until neutral pH was reached to remove residual inorganic species and subsequently dried to constant mass. The final activation conditions applied in the individual studies are summarized in **Table 5**.

Paper	Heating rate [°C/min]	Temperature [°C]	Activation time [h]	Flow rate of N_2 [cm^3/min]	Activator	Precursor: activator ratio
Biomass						
I	5	800	3	250	KOH, $K_2C_2O_4$, KOH/$K_2C_2O_4$,	1:1-1:4
Recovered carbon black from ELTs						
II	7	800-900	2	150	KOH	1:1
III	5-13	700-900	1-4	200	KOH, K_2CO_3, KCl, CH_3COOK, $K_2C_2O_4$	1:3-1:6
Recovered graphite from LiBs						
IV	5	700-900	3	250	KOH	1:5-1:7

4.3.1.1 Obtaining ACs from woody biomass

ACs were produced from biomass via chemical activation followed by thermal treatment under inert conditions. Potassium-based activating agents, including KOH, $K_2C_2O_4$, and mixed KOH/$K_2C_2O_4$ systems, were employed.

The precursor-to-activator mass ratio was systematically varied in the range of 1:1–1:4 and constituted the key manipulated parameter. Thermal activation was conducted in a tubular furnace under a constant nitrogen flow of 250 cm^3/min. A fixed heating rate of 5 °C/min, an activation temperature of 800 °C, and a residence time of 3 h were applied for all samples. These thermal parameters were kept constant, while the type of activating agent and the precursor-to-activator mass ratio were intentionally adjusted to evaluate their effect on the properties of the resulting ACs. The applied activation conditions correspond to those summarized in **Paper I**.

4.3.1.2 Obtaining ACs from recovered carbon black

Recovered carbon black derived from end-of-life tires was converted into activated carbons under potassium-assisted activation conditions using differentiated thermal protocols.

For **Paper II**, chemical activation was carried out exclusively with KOH at a fixed precursor:activator mass ratio of 1:1. Thermal treatment was performed under a nitrogen flow of 150 cm^3/min, applying a heating rate of 7 °C/min. The process temperature was varied within the range of 800–900 °C, while the activation time was maintained at 2 h. Under these conditions, the activation temperature represented the principal variable, whereas the remaining parameters were held constant.

In **Paper III**, a wider parameter space was explored. Activation was conducted using different potassium-containing reagents (KOH, K_2CO_3, KCl, CH_3COOK, and $K_2C_2O_4$), and the precursor:activator mass ratio was adjusted between 1:3 and 1:6. Thermal treatment was carried out under a nitrogen flow of 200 cm^3/min, with heating rates varied from 5 to 13 °C/min, activation temperatures between 700 and 900 °C, and residence times ranging from 1 to 4 h. In this study, the type of activating agent, thermal regime, and precursor-to-activator ratio were intentionally modified to evaluate their impact on the activation outcome and material characteristics.

4.3.1.3 Obtaining activated carbons using graphite recovered from LiBs

Recovered graphite obtained from lithium-ion batteries was converted into activated carbons through potassium-assisted chemical activation. KOH was employed as the activating agent.

Thermal activation was conducted under a continuous nitrogen flow of 250 cm^3/min, using a fixed heating rate of 5 °C/min. The activation temperature varied between 700 and 900 °C, while the residence time was maintained at 3 h for all samples. The graphite-to-activator mass ratio constituted a key manipulated parameter and was adjusted within the range of 1:5–1:7 to assess its influence on the activation outcome. Under these conditions, the activation temperature and precursor-to-activator ratio were systematically varied, whereas the remaining process parameters were kept constant. The applied activation conditions correspond to those summarized in **Paper IV**.

4.3.2 CO_2 adsorption studies

4.3.2.1 CO_2 capture performance

In **Papers I** and **II**, the ability of biomass- and recovered carbon black–derived activated carbons to adsorb CO_2 was examined. Gas uptake measurements were carried out at specific temperatures ranging from 0 to 30 °C, with pressure reaching up to 1 bar. Before analysis, the samples were conditioned by evacuation under high vacuum to eliminate residual moisture and adsorbed gases.

4.3.2.2 CO_2/N_2 selectivity

In **Papers I** and **II**, the ideal adsorption solution theory (IAST) was utilized to calculate the selectivity for CO_2/N_2 adsorption of the ACs, which is considered a critical parameter for CO_2 capture with reference to N_2 sorption data at 25 °C.

In **Paper I**, selectivity trends were examined as a function of total pressure under a fixed CO_2 molar fraction of 0.05, representing a particularly demanding scenario for sorbent-based systems, as well as across varying CO_2 concentrations. In **Paper II**, the IAST-based evaluation was further applied to equimolar CO_2/N_2 mixtures and gas compositions relevant to post-combustion capture conditions (15% CO_2 and 85% N_2).

4.3.2.3 Cyclic performance

Cyclic regeneration stability was investigated in both **Paper I** and **Paper II** to evaluate the durability and reusability of the adsorbents under repeated operation. In **Paper I**, regeneration performance was assessed over 1–20 consecutive adsorption–desorption cycles, whereas in **Paper II** the evaluation was conducted over 1–10 cycles, reflecting sustained performance under cyclic working conditions.

5. Results and discussion

The present chapter is organized according to a cause–effect framework that links material design to adsorption performance. The discussion follows the sequence: selection of precursor and activating agent → activation pathway and evolution of the carbon microstructure → development of porosity and surface accessibility → changes in surface chemistry → adsorption response (capacity, selectivity, cyclic stability).

The chosen approach is necessary because, in carbon-based materials, CO_2 capture efficiency is not a simple function of high BET surface area. Instead, adsorption performance arises from the matching of pore size and adsorption energetics to the CO_2 molecule, as well as from the balance between microporosity and mass transport resistance. At the same time, the waste streams investigated in this work (biomass, rCB from waste tires, and graphite from LiBs) differ substantially in structural ordering of carbon atoms, heteroatom content, and mineral impurities. Consequently, the same activating agent may lead to different structural reconstruction pathways and pore development mechanisms.

Based on these considerations the present chapter is structured around three main parts: (I) activation-driven pore development and carbon framework evolution; (II) surface chemistry and potassium-assisted activation mechanisms; and (III) adsorption performance evaluation for CO_2 capture (where applicable). The investigation of textural and structural properties constitutes the first level of material screening, since pore size distribution, microporosity, and carbon framework ordering govern surface accessibility and adsorption energetics under post-combustion conditions. In parallel, surface chemical characteristics are analyzed to clarify how potassium-based activation modifies functional groups and regulates gas–solid interactions. Finally, CO_2 uptake, CO_2/N_2 selectivity, and cyclic stability are discussed for systems where adsorption measurements were performed (**Papers I–II**), whereas the remaining studies **(Papers III–IV**) are interpreted in terms of their contribution to scalable production routes and structure–property relationships.

This structure directly reflects the sequential precursor-to-performance pathway adopted in this dissertation. **Figure 16** summarizes how each part contributes to material screening and application-oriented assessment.

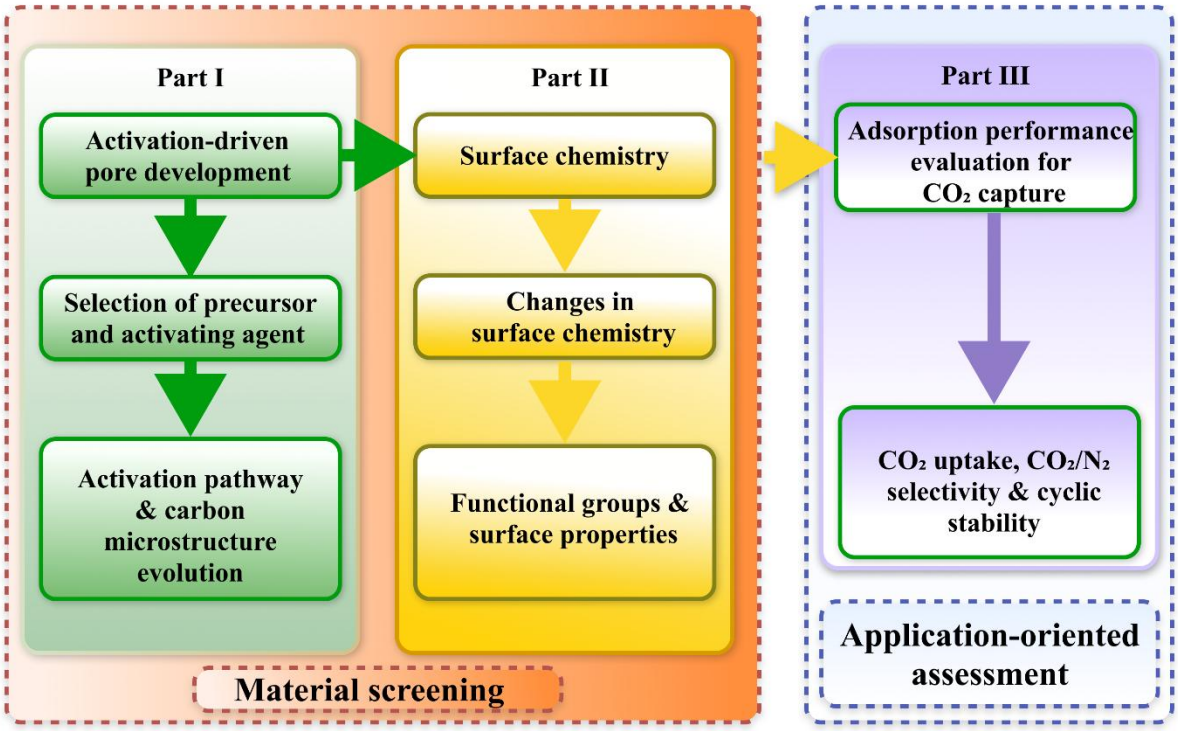

Figure 16. Framework illustrating material design, and performance connect to application-oriented assessment.

5.1 Activation and the development of porosity and carbon framework structure

This section analyzes activation-driven pore development and carbon framework reconstruction using KOH as a common reference activating agent (**Papers I–IV**). The discussion focuses on how precursor origin and activation parameters, particularly temperature and precursor-to-KOH mass ratio, influence porosity evolution and structural transformations, thereby enabling direct comparison of reactivity and pore formation pathways in waste-derived carbon materials.

5.1.1 Precursor as a determinant of reactivity

Biomass-derived carbon (**Paper I**) exhibited the highest activation responsiveness among the studied waste streams. Increasing the biomass-to-KOH ratio from 1:1 to 1:4 led to a systematic increase in BET surface area and total pore volume from approximately 1956 to

2655 $m^2\ g^{-1}$ (~36%) and from 0.943 to 1.339 $cm^3\ g^{-1}$ (~42%), respectively, with micropore volumes (< 2 nm) exceeding 1.0 $cm^3\ g^{-1}$ at moderate activation severities (1:2–1:3). At higher KOH loading, further surface area growth was accompanied by pore widening and a pronounced decrease in material yield, indicating the onset of over-etching. XRD analysis corroborated this trend by revealing progressive broadening and attenuation of the (002) basal plane reflection (2θ = 19.3–22.7°) and the overlapping (100)/(101) in-plane reflections (2θ = 43–44°), which indicated increasing turbostratic disorder and fragmentation of graphene layers.

Recovered carbon black, investigated in **Paper II** and **Paper III**, exhibited substantially lower reactivity toward KOH activation. Even under aggressive conditions used in **Paper III** (rCB:KOH ratios up to 1:6 and temperatures up to 900 °C), micropore volumes remained limited (≤ 0.332 $cm^3\ g^{-1}$), while mesoporosity dominated the pore structure, with total pore volumes approaching ~0.9 $cm^3\ g^{-1}$ and BET surface areas reaching approximately 1000 $m^2\ g^{-1}$. Furthermore, Raman analysis revealed high defect densities (I_D/I_G = 1.04–1.07), indicating a strongly disordered structure; however, extensive micropore network formation remained restricted. This behavior reflected the structurally compact nature of rCB, which limited effective structural reconstruction and favored pore widening over dense micropore formation.

Recovered graphite from LiBs (**Paper IV**) represented the most structurally resistant precursor among the investigated systems. Measurable porosity developed only under high activation severity (graphite:KOH ratios of 1:4–1:6 and temperatures of 700–900 °C), yielding BET surface areas in the range of approximately 531–678 $m^2\ g^{-1}$ and total pore volumes between 0.286 and 0.442 $cm^3\ g^{-1}$. XRD patterns indicated preservation of graphitic ordering after activation, while Raman spectroscopy revealed a pronounced increase in defect density, with the I_D/I_G ratio rising from 0.251 to 1.053. This combination suggests that KOH activation primarily induced localized defect formation and edge disorder rather than complete lattice collapse.

Comparison of the three materials showed that KOH activation produced distinct pore development pathways governed by precursor characteristics. Biomass formed dense microporous networks but became susceptible to over-etching at high activation severity, recovered carbon black underwent moderate transformation dominated by mesopore formation, and recovered graphite exhibited the greatest structural resistance, requiring aggressive conditions to initiate framework reconstruction. Consequently, precursor selection emerged as a key factor controlling porosity evolution and structural stability in waste-derived activated carbons. A comparative summary of textural properties and activation response is provided in **Table 6**.

Table 6. Activation and structural response of investigated waste-derived carbon precursors under KOH treatment.

Precursor (Paper)	**Activation conditions (precursor: KOH ratio, temperature)**	**BET surface area ($m^2\ g^{-1}$)**	**Total pore volume ($cm^3\ g^{-1}$)**	**Micropore volume ($cm^3\ g^{-1}$)**	**Dominant pore regime**	**XRD response**	**Raman response (I_D/I_G)**	**Structural implication**
Biomass (Paper I)	1:1–1:4, 800 °C	1956–2655	0.943–1.339	0.836-1.021	Microporous	Broadening and attenuation of (002) and (100)/(101)	Not measured	Turbostratic disorder and layer fragmentation
rCB (Papers II–III)	1:1–1:6, 700–900 °C	131–1025	0.275–0.901	0.036-0.327	Mesoporous -dominated	Limited framework reconstruction	1.04–1.07	Defective but compact carbon matrix
Recovered graphite (Paper IV)	1:4–1:6, 700-800 °C	531–678	0.286–0.442	~0.20	Mixed micro/mesoporous	Preservation of graphitic peaks	0.251 → 1.053	Defect generation with retained long-range order

5.1.2 Relevance of porosity beyond BET surface area

Across the investigated materials, pore size distribution analysis highlighted that the development of narrow micropores (0.3 to 1.0 nm), specifically ultramicropores (<0.7 nm), was a key structural feature influencing CO_2 adsorption in the systems where adsorption measurements were performed.

In biomass-derived ACs (**Paper I**), KOH activation generated a dense population of micropores below 1.25 nm based on N_2-derived PSD and a pronounced fraction of ultramicropores and supermicropores (0.7–2 nm) based on CO_2-derived PSD, with dominant peaks in the 0.3–1.0 nm range. According to widely reported adsorption mechanisms in porous carbons, these pore dimensions closely match the kinetic diameter of CO_2 (~0.33 nm**)** and maximize adsorption potential at low partial pressures, providing a structural basis for the high uptake observed in this system.

rCB-derived ACs evaluated for CO_2 adsorption (**Paper II**) exhibited broader N_2-derived PSD profiles dominated by mesopores, with micropores concentrated in the 1.05–1.54 nm range and mesopores spanning 2.30–34.05 nm. CO_2-derived PSD confirmed ultramicropores at 0.37–0.59 nm with additional contributions at 0.61–0.91 nm; however, their limited volumetric fraction relative to mesoporosity was consistent with the lower CO_2 adsorption performance compared to biomass-derived carbons, in agreement with trends reported for mesopore-rich ACs. A similar structural pattern was observed in rCB samples optimized for KOH activation (**Paper III**), where micropores accounted for ~30–40% of the total pore volume, with dominant populations centered at 0.99–1.63 nm and mesopores distributed between 2.0 and 13.49 nm. Despite increased micropore contribution, pore widening remained significant, providing structural context for the CO_2 adsorption limitations observed in rCB-based systems.

For the remaining system, recovered graphite (**Paper IV**), PSD analysis primarily served as a structural screening tool because CO_2 uptake measurements were not performed. KOH activation induced partial formation of micropores below 2 nm, with pronounced PSD peaks between 1.2 and 2.0 nm, while mesopores remained predominantly in the 2.2–4.0 nm range. These results reinforce that the presence and distribution of narrow micropores constitute a critical structural descriptor for CO_2 adsorption performance where measured, whereas PSD analysis in non-tested systems provides guidance for identifying promising activation pathways requiring further experimental validation (**Table 7**).

Table 7. Pore size distribution characteristics and CO_2 adsorption relevance.

Precursor (Paper)	PSD method	Dominant micropore range (nm)	Narrow micropore range (<0.7 nm)	Dominant mesopore range (nm)	Structural implication	CO_2 adsorption measured
Biomass (Paper I)	N_2 + CO_2 DFT	<1.25 (N_2)	High: 0.3–1.0 (CO_2)	2.1–4.0	Dense microporous network	Yes
rCB (Paper II)	N_2 + CO_2 DFT	1.05–1.54 (N_2)	Limited: 0.37–0.59; 0.61–0.91 (CO_2)	2.3–35	Mesoporosity dominates, limited effective micropore fraction	Yes
rCB optimized (Paper III)	N_2 DFT	0.99–1.63 (N_2)	Not resolved separately	2.0–13.5	Moderate micropore enhancement, pore widening dominates	No
Recovered graphite (Paper IV)	N_2 DFT	1.2–2.0 (N_2)	Present (cumulative volume evidence)	2.2–4.0	Micropore-dominant structure with persistent mesoporosity	No

5.1.3 Morphology and activator diffusion as mechanistic factors

Beyond chemical reactivity and lattice-level reconstruction, particle morphology and activator transport were identified as additional controlling factors governing pore development during potassium-assisted activation. SEM analysis enabled direct visualization of precursor-dependent differences in terms of particle shape, aggregation state, and surface accessibility, which are widely recognized in the literature as key parameters affecting alkali metal diffusion and spatial activation uniformity [51].

Biomass-derived carbons (**Paper I**) exhibited highly open and interconnected porous morphologies after KOH activation, characterized by thin pore walls and extensive framework etching. Such open architectures facilitated rapid potassium penetration and promoted relatively homogeneous activation throughout the carbon matrix, in agreement with previous reports on lignocellulosic precursors [90]. At higher activation severity, however, the same efficient transport pathways accelerated carbon consumption, leading to framework thinning and the onset of over-etching.

rCB-derived carbons (**Papers II and III**) consisted of rigid, spherical primary particles forming compact aggregates. SEM analysis revealed a closed and clustered morphology that restricted potassium diffusion into particle interiors and promoted surface-localized reactions. As a consequence, activation proceeded in a spatially heterogeneous manner, favoring pore widening and mesopore formation rather than the development of dense, interconnected microporous networks.

Recovered graphite (**Paper IV**) displayed plate-like, highly ordered particles prior to activation. Following KOH treatment, SEM micrographs revealed pronounced surface roughening, defect formation, and partial fragmentation, while remnants of the layered graphitic structure remained visible. This morphological evolution indicated selective etching dominated by reactions at edges, grain boundaries, and defect sites rather than uniform bulk restructuring.

Taken together, these observations demonstrated that precursor morphology directly influenced activator accessibility and diffusion efficiency, thereby regulating the balance between homogeneous pore generation, localized surface etching, and framework preservation during KOH activation (**Table 8**). Consequently, effective pore engineering in waste-derived carbons required simultaneous consideration of activation chemistry and morphology-induced mass transport limitations.

Table 8. Morphological features and potassium diffusion behavior.

Precursor (Paper)	Morphological features (SEM)	KOH accessibility	Activation uniformity	Mechanistic implication	Morphology
Biomass (Paper I)	Open interconnected porous framework	High	Homogeneous	Rapid micropore generation, prone to over-etching	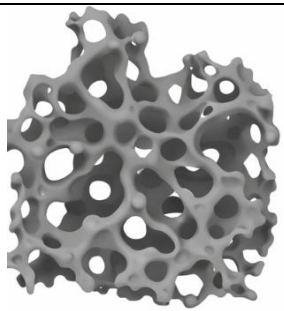
rCB (Papers II–III)	Rigid spherical particles, compact aggregates	Limited	Heterogeneous	Surface-localized reactions, mesopore formation dominates	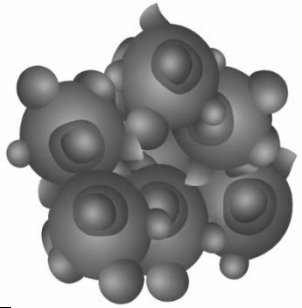
Recovered graphite (Paper IV)	Plate-like layered particles	Moderate (edge sites)	Localized	Selective etching and carbon framework preservation	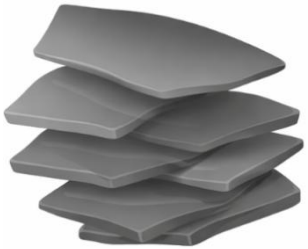

5.2 Variability of activation mechanisms and CO_2-specific surface chemistry among potassium-based activators

This section examines the variability of activation mechanisms among potassium-based activating agents by comparing their roles in pore development and carbon framework modification (**Papers I and III**), as well as the associated evolution of surface chemistry in systems where adsorption performance was evaluated (**Papers I and II**). The analysis focuses on how potassium precursor speciation, thermal decomposition behavior, and in situ potassium migration controlled etching efficiency, pore formation, structural expansion, and functional group development.

Within the current framework, differences between KOH and potassium salts were evaluated for biomass-derived carbons in **Paper I** (comparison between KOH and $K_2C_2O_4$) and for rCB-derived carbons in **Paper III** (comparison between KOH, K_2CO_3, CH_3COOK, $K_2C_2O_4$, and KCl), and were attributed to distinct reaction pathways and pore generation efficiencies.

For systems with available CO_2 adsorption data (**Paper I and Paper II**), the surface chemistry of KOH-activated carbons and $K_2C_2O_4$-activated biomass carbons (**Paper I**) was evaluated in relation to adsorption behavior, where surface functional groups were treated as secondary modifiers of gas–solid interactions acting in combination with micropore structure rather than as primary performance drivers. For recovered graphite (**Paper IV**), surface chemical characterization was used to interpret activation-induced structural modification instead of adsorption performance due to the absence of CO_2 uptake measurements.

5.2.1 KOH vs. K-based salts: reactivity and transport related limitations in activation efficiency

The comparison between KOH and $K_2C_2O_4$ in **Paper I** demonstrated clear differences in activation behavior arising from differences in potassium reactivity and transport properties in biomass-derived ACs. Under identical activation conditions (mass ratio biomass:activator = 1:4, 800 °C), KOH produced substantially higher overall porosity, with a BET surface area of 2655 $m^2\ g^{-1}$ and total pore volume of 1.339 $cm^3\ g^{-1}$, whereas $K_2C_2O_4$ yielded lower values (1709 $m^2\ g^{-1}$ and 0.885 $cm^3\ g^{-1}$, respectively). Despite this difference, both activators generated comparable CO_2 accessible narrow micropore volumes relevant for CO_2 adsorption (0.133 $cm^3\ g^{-1}$ for KOH and 0.150 $cm^3\ g^{-1}$ for $K_2C_2O_4$), indicating that KOH primarily enhanced bulk pore expansion, while $K_2C_2O_4$ promoted more selective formation of narrow micropores. This distinction was further reflected in pore structure distribution and material yield. KOH

activation generated a larger mesopore contribution (0.318 $cm^3\ g^{-1}$) and resulted in significant carbon burn-off (7.8%), whereas $K_2C_2O_4$ produced a more micropore-focused structure with limited mesoporosity (0.091 $cm^3\ g^{-1}$) and higher yield (18.5%). SEM observations supported these trends by revealing uniformly etched, highly open frameworks for KOH-activated carbon and localized cracking with compact granular regions for $K_2C_2O_4$-activated sample, indicating restricted potassium mobility.

Furthermore, XRD analysis of unwashed samples showed that $K_2C_2O_4$ activation favored the formation of crystalline carbonate-rich potassium phases ($K_2CO_3 \cdot 1.5H_2O$, $K_4H_2(CO_3)_3 \cdot 1.5H_2O$, K_2CO_3, K_2O), which is in agreement with literature reports on $K_2C_2O_4$ decomposition behavior [91]. KOH-activated samples exhibited broader and less intense potassium-related reflections, indicating the presence of ess crystalline and weakly bound potassium species. This difference reflects higher potassium mobility and reactivity during KOH activation, enabling homogeneous framework etching and efficient pore generation, whereas oxalate-based activation remains governed by diffusion-limited and structurally conservative mechanisms (**Table 9**).

Table 9. Comparison of KOH and $K_2C_2O_4$ activation for biomass-derived carbons (**Paper I**).

Parameter	**KOH activation**	**$K_2C_2O_4$ activation**
Potassium reactivity	Intensive carbon etching	Lower reactivity with carbonate-dominated decomposition products
Potassium transport	Homogeneous penetration	Restricted transport with localized activation zones
Pore development pathway	Strong bulk pore expansion and framework thinning	Selective formation of narrow micropores with limited pore widening
Carbon yield	Low	Higher
Structural implication	Efficient but aggressive activation	Milder, transport-limited activation

The screening of potassium-based activators in **Paper III** demonstrated that pore development in rCB-derived carbons was strongly influenced by potassium speciation and transport behavior. KOH exhibited the highest activation efficiency, reaching S_{BET} = 945 m² g⁻¹, V_{TOT} = 0.743 cm³ g⁻¹, and $V_{MIC(N_2)}$ = 0.303 cm³ g⁻¹. Among the potassium salts, $K_2C_2O_4$ showed the strongest performance, with S_{BET} = 299 m² g⁻¹, V_{TOT} = 0.369 cm³ g⁻¹, and $V_{MIC(N_2)}$ = 0.093 cm³ g⁻¹, while CH_3COOK (S_{BET} = 217 m² g⁻¹, V_{TOT} = 0.240 cm³ g⁻¹, $V_{MIC(N_2)}$ = 0.071 cm³ g⁻¹) and K_2CO_3 (S_{BET} = 146 m² g⁻¹, V_{TOT} = 0.207 cm³ g⁻¹, $V_{MIC(N_2)}$ = 0.043 cm³ g⁻¹) produced lower values. KCl exhibited negligible textural properties development, resulting in the overall activation efficiency trend: KOH > $K_2C_2O_4$ > CH_3COOK > K_2CO_3 > KCl. Furthermore, SEM–EDS analysis in **Paper III** revealed systematic differences in potassium distribution among the activators. KOH produced the highest potassium loading (~29.5 wt%) with a relatively homogeneous spatial distribution, consistent with efficient potassium transport and uniform activation. $K_2C_2O_4$ exhibited high potassium content (~27.5 wt%) accompanied by patchy spatial distribution, whereas CH_3COOK (~20.9 wt%) and K_2CO_3 (~13.1 wt%) showed increasingly heterogeneous potassium dispersion and localized potassium-rich regions. This behavior directly correlated with the resulting textural properties, as activators with more uniform potassium distribution generated higher surface area and micropore volume. Overall, these results demonstrate that effective activation of rCB requires not only sufficient potassium availability but also homogeneous potassium transport within the carbon matrix, conditions most efficiently fulfilled by KOH and only partially achieved by potassium salts, as summarized in **Table 10**.

Table 10. Summary of potassium-speciation-controlled activation behavior in rCB-derived carbons (**Paper III**).

Activator	Potassium transport behavior	Spatial K distribution	Pore formation tendency	Overall activation effectiveness
KOH	High mobility	Homogeneous	Strong	Highest
$K_2C_2O_4$	Moderate mobility	Patchy	Moderate	Intermediate
CH_3COOK	Limited mobility	Heterogeneous	Weak	Low
K_2CO_3	Low mobility	Strongly heterogeneous	Very weak	Very low
KCl	Minimal chemical interaction	Poor penetration	Negligible	Ineffective

A central outcome of the K-based activator comparison in **Paper I** and **Paper III** is that effective activation requires chemically reactive potassium species, sufficient potassium mobility with homogeneous distribution during heating, and controlled pore development without excessive burn-off. In this context, the differences observed between KOH and potassium salts (K_2CO_3, CH_3COOK, $K_2C_2O_4$, KCl) reflect distinct reaction pathways and potassium transport efficiencies. KOH consistently exhibited the highest activation efficiency in both biomass- and rCB-derived systems due to its strong interaction with the carbon matrix, while simultaneously introducing a process-level trade-off associated with increased carbon consumption at high activation severity. Consequently, for KOH activation, the identification of an optimal activation window that balances overall porosity development, BET surface area, and structural stability emerges as a key design criterion for the development of practical adsorption-oriented sorbents.

5.2.2 Surface chemistry evolution during K-based activation and its role in CO_2 adsorption

Surface chemistry analysis across the investigated systems indicates that potassium-based activation introduces a broadly similar set of oxygen-containing functional groups; however the relative abundance and chemical environment of these groups depend on the activating agent and precursor type.

In biomass-derived carbons (**Paper I**), both KOH and $K_2C_2O_4$ produced comparable FT-IR spectra with bands assigned to –C–H, –O–H, –C=O, –C–O, –C=C, and –C≡C functionalities, indicating that the same types of surface functional groups are present irrespective of the activator, although their relative abundance may differ. However, XPS analysis revealed that KOH exerted a stronger influence on surface reconstruction, promoting higher concentrations of oxygen functionalities (–C=O, –C–O) and defect-rich aromatic domains, whereas $K_2C_2O_4$ favored partial retention of carbonate-related species (CO_3^{2-}), in agreement with the XRD detection of potassium carbonate phases ($K_2CO_3 \cdot 1.5H_2O$, $K_4H_2(CO_3)_3 \cdot 1.5H_2O$, and K_2CO_3). In mixed activation systems (KOH/$K_2C_2O_4$), KOH dominated the resulting surface chemistry, confirming its stronger chemical interaction with the carbon matrix.

For rCB-derived carbons activated with KOH (**Paper II**), FT-IR analysis similarly confirmed the presence of –O–H, and –C–O functionalities, which are known to enhance CO_2 adsorption through increased quadrupole–dipole interactions. In these systems, oxygen-

containing surface functionalities were therefore treated as secondary contributors, with textural properties considered the primary factor controlling CO_2 adsorption capacity.

In recovered graphite activated with KOH (**Paper IV**), XPS results showed an increase in the graphitic carbon contribution accompanied by partial redistribution of surface oxygen species, including –C–O, –O–H, and –C=O groups. This behavior reflects K intercalation and high-temperature redox reactions, which restructure the carbon framework while modifying the population and distribution of oxygen-containing functionalities. Although CO_2 adsorption was not evaluated for this system, the increase in graphitic ordering together with the reorganization of surface oxygen species suggests that the CO_2 adsorption performance would be primarily determined by the developed microporosity and could therefore be expected to follow trends similar to those observed for other KOH-activated carbons with comparable textural properties.

These results demonstrate that potassium-based activation generates broadly similar functional group families across different precursors and KOH induces the most pronounced surface chemical restructuring. In systems relevant to CO_2 capture (**Paper I** and **Paper II**), surface chemistry acts primarily as a supporting factor that enhances adsorption energetics in combination with appropriate pore architecture, rather than serving as the dominant performance-controlling parameter. A consolidated overview of the surface chemical transformations induced by the different potassium activators is presented in **Table 11**.

Table 11. Comparison of surface chemistry evolution with different potassium-based activation.

System (Paper)	Activator	Dominant surface features	Activator influence on surface chemistry	CO_2 relevance
Biomass-derived ACs (Paper I)	KOH	–C=O, –C–O, –O–H groups, defect-rich aromatic domains	Strong surface reconstruction and enhanced defect formation	Contributing factor alongside pore development
Biomass-derived ACs (Paper I)	$K_2C_2O_4$	Similar to KOH functional group types, partial carbonate retention	Milder chemical modification and carbonate stabilization	Supporting role; less pronounced than structural effects
rCB-derived ACs (Paper II)	KOH	O–H, and –C–O groups	Moderate surface oxidation coupled with pore development	Limited direct contribution
Recovered graphite (Paper IV)	KOH	Increased graphitic carbon fraction, C–O, –O–H, and –C=O groups	Framework restructuring via K intercalation and redox reactions	Mechanistic relevance only

5.3 CO_2 adsorption performance and CO_2/N_2 separation behavior

This section analyzes the CO_2 capture performance and selectivity behavior of waste-derived activated carbons by integrating adsorption capacity, selectivity, and cyclic stability results obtained in **Paper I** and **Paper II**. The discussion focuses on how precursor type, activation strategy, and resulting pore structure influence adsorption behavior under low-pressure conditions (≤1 bar) relevant to post-combustion CO_2 capture. Within this framework, biomass-derived carbons (**Paper I**) and recovered carbon black–derived carbons (**Paper II**) are chosen to compare structure–performance relationships controlling CO_2 uptake and CO_2/N_2 selectivity.

5.3.1 CO_2 adsorption capacity and temperature-dependent performance

In **Paper I**, biomass-derived activated carbons exhibited steep low-pressure CO_2 uptake, confirming adsorption dominated by narrow micropores. The highest capacity was obtained for KOH-activated material at low KOH loading (biomass:KOH = 1:1), reaching 5.95 mmol g^{-1} at 25 °C and 9.65 mmol g^{-1} at 0 °C. Increasing the KOH ratio reduced CO_2 uptake despite higher BET surface area and total pore volume, as the CO_2-accessible micropore volume decreased from 0.164 to 0.133 cm^3 g^{-1}, indicating pore widening and partial loss of micropores below 1.4 nm. $K_2C_2O_4$-activated biomass (biomass:$K_2C_2O_4$ = 1:4) achieved comparable uptake (5.52 mmol g^{-1} at 25 °C and 8.79 mmol g^{-1} at 0 °C) at lower S_{BET}, V_{TOT}, and $V_{MIC(N2)}$, demonstrating that selective formation of narrow micropores is more critical for CO_2 capture than maximizing total porosity.

In **Paper II**, rCB-derived carbons showed pronounced temperature-dependent adsorption behavior characteristic of physisorption. KOH-activated rCB exhibited a CO_2 uptake, reaching 30.9 cm^3 g^{-1} (1.38 mmol g^{-1}) at 0 °C and 20.5 cm^3 g^{-1} (0.84 mmol g^{-1}) at 25 °C under 1 bar. Textural analysis in **Paper II** further supports the interpretation of the activation process. Increasing the KOH activation temperature from 800 to 900 °C resulted in systematic enhancement of pore development, with BET surface area increasing from 131 to 328 m^2 g^{-1} and total pore volume from 0.275 to 0.448 cm^3 g^{-1}. This evolution was driven mainly by micropore formation, with micropore volume increasing from 0.036 to 0.100 cm^3 g^{-1}. Importantly, both supermicropores and ultramicropores increased with temperature (0.021 → 0.069 cm^3 g^{-1} and 0.015 → 0.031 cm^3 g^{-1}, respectively), indicating improved development of CO_2-relevant narrow porosity. It should be noted that CO_2 adsorption measurements were performed only for the 900 °C-activated sample; therefore, the textural trends at lower

temperatures are interpreted as indicators of adsorption potential rather than direct performance metrics.

Cyclic stability tests in both studies demonstrated excellent regenerability of the surfaces. In **Paper I**, KOH- and $K_2C_2O_4$-activated biomass carbons maintained constant CO_2 uptake over 20 adsorption–desorption cycles at 25 °C, with a maximum deviation of approximately 0.09 mmol g^{-1}. Similarly, in **Paper II**, KOH-activated rCB showed no measurable capacity loss over 10 cycles at 0 °C. The preserved performance confirms reversible physisorption within structurally stable micropores and indicates the absence of irreversible surface reactions during repeated operation.

These results show that high CO_2 uptake combined with long-term cyclic stability is achieved when the activation conditions promote the formation of stable narrow microporosity as the key structural parameter controlling adsorption performance in waste-derived activated carbons.

Table 12. Structural and functional comparison of the performance of waste-derived adsorbents (**Paper I** and **Paper II**).

Precursor type (Paper)	**Activator (precursor:KOH ratio, and temperature)**	**Key pore feature**	**Structural characteristics of precursor**	**Performance implication**
Biomass (Paper I)	KOH (biomass:KOH = 1:1, 800 °C)	High narrow micropore density	Highly disordered lignocellulosic carbon framework	Strong low-pressure CO_2 adsorption driven by narrow micropores
Biomass (Paper I)	$K_2C_2O_4$ (biomass:KOH = 1:4, 800 °C)	Similar but less developed narrow micropore region compared to KOH	Moderately preserved carbon framework	Efficient CO_2 uptake despite lower S_{BET}, V_{TOT}, and $V_{MIC(N2)}$
Recovered carbon black (Paper II)	KOH (rCB:KOH = 1:1, 900 °C)	Mixed micro/mesoporous structure	Compact, thermally pre-processed aggregated particles	Low CO_2 uptake because of structural limitations

5.3.2 CO_2/N_2 selectivity and separation performance

CO_2/N_2 selectivity was evaluated using IAST calculations for biomass-derived carbons (**Paper I**) and rCB-derived carbons (**Paper II**) under dilute and post-combustion–relevant conditions. In **Paper I**, all investigated materials exhibited selectivity values above 12 at low CO_2 mole fraction (0.05) and at 1 bar, confirming effective separation performance under these selected conditions. The highest selectivity was obtained for the $K_2C_2O_4$-activated carbon (20.5–21.7), whereas the KOH-activated sample (biomass:KOH = 1:1) exhibited slightly lower values (19.13–21.29). Increasing the KOH loading (biomass:KOH = 1:4) reduced the selectivity (12.8–13.8) due to the partial loss of ultramicropores. In addition, the $K_2C_2O_4$-derived carbon demonstrated robust performance under variable feed compositions, maintaining selectivity above 20 across the entire range of CO_2 concentrations and operating pressures. These trends indicate that CO_2/N_2 separation efficiency is based on primarily by the availability of ultramicropore formation that preferentially accommodate CO_2 molecules while restricting N_2 adsorption due to size exclusion and enhanced adsorption potential at low pressure.

In **Paper II**, KOH-activated rCB exhibited exceptionally high selectivity for an equimolar CO_2/N_2 mixture at low pressure (>300 at 0.001 bar) and maintained favorable performance under flue-gas conditions (~60 at 1 bar, 15% CO_2). This behavior, evaluated from the coefficient of determination (R^2) as a function of the cumulative micropore volume within defined pore width ranges, is mainly associated with submicropores and ultramicropores. The preferential filling of these narrow pores at low pressure leads to outstanding separation, while their progressive occupation at higher pressure results in a decrease in selectivity, although the values remain competitive for practical applications.

Taken together, the findings indicate that CO_2/N_2 selectivity is primarily determined by the ultramicropore size matching, providing the strongest structural contribution to separation performance across both precursor systems, as summarized in **Table 13**.

Table 13. Comparison of CO_2/N_2 selectivity behavior for waste-derived activated carbons (**Paper** I and **Paper II**).

Precursor type	**Activator (biomass:KOH ratio/temperature)**	**Process conditions**	**Dominant selectivity driver**	**Selectivity behavior**	**Separation implication**
Biomass (Paper I)	KOH (biomass:KOH = 1:1)	Low CO_2 fraction (0.05), ≤1 bar	High ultramicropore density	High selectivity	Favorable for dilute CO_2 separation
Biomass (Paper I)	$K_2C_2O_4$ (biomass: $K_2C_2O_4$ = 1:4)	Low CO_2 fraction (0.05), ≤1 bar	Refined ultramicropores	The highest selectivity	Robust performance under variable feed compositions
Biomass (Paper I)	KOH (biomass: KOH = 1:4)	Low CO_2 fraction (0.05), ≤1 bar	Partial ultramicropore loss	Reduced selectivity	Over-activation limits separation efficiency
rCB (Paper II)	KOH (900 °C)	Low pressure and flue-gas composition	Strong CO_2 confinement in submicropores and ultramicropores	Very high selectivity at low pressure and high values at flue gas conditions	Suitable for post-combustion capture conditions

6. Conclusions

This thesis investigates the transformation of carbon-intensive waste streams into functional porous materials for CO_2 capture within a circular materials framework. The work aims to establish a methodology for the valorization of structurally diverse carbon residues into high-performance sorbents through chemically controlled activation. Potassium-assisted activation was applied to three waste-derived carbon precursors, namely woody biomass, recovered carbon black from end-of-life tires, and graphite from spent lithium-ion batteries, and the resulting materials were evaluated for their gas sorption performance under physisorption dominated conditions where adsorption data were available. The major conclusions are summarized as follows:

- **Waste-stream valorization into functional sorbents**

The work shows that precursor origin governs activation response, attainable pore architecture, and structural stability (**Papers I–IV**).

Woody biomass, rCB, and recovered graphite were demonstrated as viable precursors for producing activated carbons through potassium-mediated chemical activation, establishing a unified waste-to-sorbent framework aligned with circular economy principles and carbon intensive waste management strategies.

- **Precursor-dependent activation responsiveness controls pore development**

The results revealed a precursor-dependent activation behavior, indicating that a universal response could not be assumed for structurally diverse waste-derived carbons. Each material exhibited a different degree of responsiveness under identical potassium-based activation conditions. This variation was attributed to differences in the structural organization of the carbon framework and the resulting accessibility of reactive carbon domains.

Biomass exhibited the highest reactivity toward KOH activation, enabling dense microporous networks and very high surface areas, but also susceptibility to over-etching at high activation severity (**Paper I**). rCB showed moderate activation responsiveness, with mesopore-dominated structures resulting from diffusion-limited activation within compact aggregates (**Papers II–III**). Recovered graphite showed the greatest structural resistance,

with porosity forming mainly through defect-driven edge etching rather than uniform framework reconstruction (**Paper IV**).

- **Microporosity governs CO_2 capture more strongly than total surface area**

The present study demonstrated that pore size distribution, rather than overall surface area, is the dominant structural descriptor influencing CO_2 capture efficiency. Specifically, narrow micropores emerged as the critical structural parameter governing selective low-pressure adsorption.

In the evaluated systems where adsorption was measured, CO_2 uptake and CO_2/N_2 selectivity correlated with the availability of narrow micropores, particularly ultramicropores, rather than with BET surface area alone.

Biomass-derived carbons achieved the highest low-pressure CO_2 capacities due to dense sub-nanometer pores (**Paper I**), whereas rCB-derived carbons showed lower uptake consistent with a smaller fraction of CO_2-relevant microporosity (**Paper II**).

- **Potassium activator chemical speciation determines activation efficiency**

The present study demonstrated that activation efficiency is not solely dictated by potassium content but by its chemical form. Variations in potassium speciation resulted in distinct activation pathways, ranging from aggressive pore expansion (KOH) to selective micropore development with improved yield retention ($K_2C_2O_4$).

KOH consistently delivered the strongest activation effect due to high potassium reactivity and relatively uniform migration within the carbon matrix, enabling efficient pore generation (**Papers I–III**). Alternative potassium salts produced milder activation, with $K_2C_2O_4$ demonstrating selective narrow micropore formation and improved yield retention in biomass-derived systems, highlighting a trade-off between aggressive pore expansion and structural conservation (**Paper I**).

- **Morphology and diffusion limitations regulate activation pathways**

This work demonstrates that precursor morphology governs activation pathways by controlling potassium transport within the carbon matrix. Structural organization and

particle compactness dictate the balance between homogeneous pore development and localized over-etching.

SEM analysis revealed that open biomass-derived structures promoted homogeneous activation but accelerated burn-off at high severity (**Paper I**). Aggregated rCB particles restricted potassium transport, favoring localized reactions and mesopore formation (**Papers II–III**). Plate-like graphite structures underwent selective edge etching with partial retention of graphitic ordering (**Paper IV**). These findings confirm that morphology-induced transport limitations are critical factors in pore engineering.

- **Surface chemistry plays a secondary but supportive role in adsorption**

The results indicate that, under physisorption-controlled conditions, adsorption performance is primarily associated with the developed micropore architecture, while surface chemistry provides a secondary contribution by modifying gas–solid interactions. Oxygen-containing functional groups therefore act as supportive modifiers rather than dominant performance-determining features.

A common feature across all materials is the potassium-driven introduction of oxygen-containing functionalities, indicating a shared activation mechanism (**Paper I** and **Paper II**). In graphite-based systems, the evolution of surface chemistry reflects potassium-induced restructuring of the carbon framework (**Paper IV**).

- **CO_2/N_2 selectivity and cyclic stability confirm separation potential**

The overall performance evaluation demonstrates that selective and stable CO_2 capture can be achieved within these structurally engineered carbon systems.

Biomass- and rCB-derived activated carbons exhibited favorable CO_2/N_2 selectivity under dilute and post-combustion conditions and maintained stable performance during repeated adsorption–desorption cycles, confirming reversible physisorption (**Papers I–II**).

7. Future outlook

Future research directions emerging from this work can be grouped into material innovation, process optimization, and application expansion, with an overarching emphasis on scalability and sustainability.

I. Material innovation

• Environmentally balanced activation strategies

Current practices for producing activated carbons through chemical activation typically require high potassium loadings and severe conditions, which lead to extensive burn-off, low material yields, and the generation of secondary waste streams. These factors reduce resource efficiency and limit the environmental sustainability of sorbent production. The development of more environmentally balanced activation strategies therefore requires approaches that enable precise pore formation while reducing chemical consumption and carbon loss. The use of alternative potassium salts, mixed-activator systems, and staged activation protocols represents a promising pathway toward the selective formation of porosity under milder conditions. In this context, the $K_2C_2O_4$-based activation of biomass-derived carbons provides an important conceptual basis for such process design (**Paper I**).

• Controlled surface functionalization

Surface chemistry in activated carbons is largely determined by the activation process itself, which limits independent control over the type, density, and spatial distribution of functional groups. Post-synthetic modification often leads to partial blockage of pores or deterioration of structural stability, resulting in reduced adsorption efficiency and poorer cyclic performance. The development of post-activation treatments that introduce tailored polar functionalities while preserving pore accessibility could therefore enhance adsorption energetics under realistic gas compositions without compromising stability. Such strategies should enable the decoupling of textural and chemical properties and provide improved performance under practical operating conditions (**Papers I–II**).

• Hybrid and composite sorbents

Waste-derived carbons in the present thesis were primarily evaluated as standalone sorbents, where adsorption performance was tuned through pore structure development and surface chemistry modification. The absence of integrated high-affinity phases limits the extent to which adsorption energetics and selectivity can be independently tailored beyond what is achievable by textural optimization alone. The development of hybrid and composite sorbents, in which waste-derived carbons are combined with high-affinity porous frameworks or functional coatings, offers a pathway to synergistic adsorption behavior by coupling the

structural robustness and conductivity of the carbon matrix with enhanced affinity toward CO_2 and other target gases (**Papers I–IV**).

II. Process optimization

- ### Mitigating diffusion limitations in compact precursors

Current activation approaches applied to compact and aggregated precursors such as rCB and graphite are limited by restricted potassium transport within dense particle structures. This results in heterogeneous activation, localized over-etching, and non-uniform micropore development, as evidenced by the spatially uneven potassium distribution and textural evolution observed in **Paper II** and **Paper IV**. Pre-conditioning strategies, including controlled particle engineering and morphology tuning prior to activation, could improve potassium accessibility and promote more homogeneous pore formation. Such approaches would enable more efficient utilization of the carbon matrix, reduce burn-off, and open pathways toward the controlled design of adsorption-relevant porosity in otherwise diffusion-limited precursors.

- ### Mechanistic refinement of potassium-assisted activation

Although potassium-assisted activation is widely applied, the mechanisms governing potassium speciation, migration, and carbon framework reconstruction remain insufficiently resolved. This limits predictive control over pore development and increases the risk of over-etching and structural degradation under severe activation conditions. Time-resolved and in situ characterization techniques could elucidate the evolution of potassium species and their interaction with the carbon matrix, enabling the rational design of activation protocols with controlled pore formation (**Papers I–III**).

- ### Dynamic and process-relevant adsorption evaluation

Most adsorption evaluations are conducted under ideal equilibrium conditions that do not adequately represent industrial gas separation environments. As a result, performance under dynamic flow, multicomponent gas mixtures, and humidity remains insufficiently understood, which limits reliable scale-up assessment. Extending the current studies toward breakthrough experiments, kinetic analysis, and humidity-influenced adsorption would bridge the gap between laboratory characterization and realistic process conditions and enable more accurate evaluation of sorbent applicability (**Papers I–II**).

III. Application expansion

- **Broadening environmental sorption applications**

Current research on waste-derived activated carbons has primarily focused on CO_2 capture, while their broader potential for environmental remediation remains largely unexplored. The tunable pore structures and adjustable surface functionalities demonstrated in this work provide a basis for extending these materials toward the removal of other gaseous pollutants and aqueous contaminants. Such expansion would enable the utilization of the same structure–property relationships identified here for a wider range of separation and purification applications (**Papers I–IV**).

- **Integration into scalable capture systems**

Most studies remain at the level of laboratory-scale evaluation of powder materials, with limited translation into reactor-relevant configurations. This gap between material synthesis and process-scale implementation prevents realistic assessment of pressure drop, mechanical stability, heat and mass transfer, and long-term operational performance. The development of shaped sorbents together with reactor-scale validation would enable the evaluation of these parameters under practical conditions and support the transfer of the most promising materials into applicable separation technologies (**Papers I–II**).

- **Sustainability and techno-economic assessment**

While the results of this thesis demonstrate the circularity potential of waste-derived sorbents, comprehensive life-cycle and techno-economic assessments are still missing. Without such analyses, the overall environmental impact and economic feasibility of large-scale implementation remain uncertain, particularly for processes integrated with tire and battery recycling infrastructure. The incorporation of life-cycle and techno-economic evaluation alongside scale-up studies would enable identification of the most resource-efficient activation strategies, optimization of material yields, and verification of the practical sustainability of the proposed value chains (**Papers II–IV**).

8. References

[1] Diejarski, B., Krzyżyńska, R., & Andersson, K. (2023). Current status of carbon capture, utilization, and storage technologies in the global economy: A survey of technical assessment. Fuel, 342, 127776. https://doi.org/10.1016/j.fuel.2023.127776

[2] IEA (2025), Global Energy Review 2025, IEA, Paris https://www.iea.org/reports/global-energy-review-2025, Licence: CC BY 4.0

[3] IEA (2019). Transforming Industry through CCUS, IEA, Paris. https://www.iea.org/reports/transforming-industry-through-ccus

[4] Hanson, E., Nwakile, C., & Hammed, V. O. (2025). Carbon capture, utilization, and storage (CCUS) technologies: Evaluating the effectiveness of advanced CCUS solutions for reducing CO_2 emissions. Results in Surfaces and Interfaces, 18, 100381. https://doi.org/10.1016/j.rsurfi.2024.100381

[5] Leonzio, G., & Shah, N. (2024). Recent advancements and challenges in carbon capture, utilization and storage. Current Opinion in Green and Sustainable Chemistry, 46, 100895. https://doi.org/10.1016/j.cogsc.2024.100895

[6] Raganati, F., & Ammendola, P. (2024). CO_2 post-combustion capture: a critical review of current technologies and future directions. Energy & Fuels, 38(15), 13858-13905. https://doi.org/10.1021/acs.energyfuels.4c02513

[7] Deng, H., Li, T., Li, H., Dang, A., & Han, Y. (2025). Carbon-based adsorbents for CO_2 capture: A systematic review. Journal of Industrial and Engineering Chemistry, 147, 39-55. https://doi.org/10.1016/j.jiec.2024.12.026

[8] Tang, S. H., Rashidi, N. A., & Lim, H. Y. (2025). Advancing biomass-based activated carbon production: challenges, techniques, and opportunities with focus on Malaysia. Environment, Development and Sustainability, 1-25. https://doi.org/10.1007/s10668-025-05998-8

[9] Ali, I., Asim, M., & Khan, T. A. (2012). Low cost adsorbents for the removal of organic pollutants from wastewater. Journal of Environmental Management, 113, 170-183. https://doi.org/10.1016/j.jenvman.2012.08.028

[10] Kundu, S., Khandaker, T., Anik, M. A. A. M., Hasan, M. K., Dhar, P. K., Dutta, S. K., ... & Hossain, M. S. (2024). A comprehensive review of enhanced CO_2 capture using activated carbon derived from biomass feedstock. RSC Advances, 14(40), 29693-29736. DOI: 10.1039/D4RA04537H

[11] Mishra, R. K., Singh, B., & Acharya, B. (2024). A comprehensive review on activated carbon from pyrolysis of lignocellulosic biomass: An application for energy and the environment. Carbon Resources Conversion, 7(4), 100228. https://doi.org/10.1016/j.crcon.2024.100228

[12] Briones-Hidrovo, A., Costa, S. M., Maganinho, C., Silva, C. M., Rocha, J., Dias, A. C., ... & Silva, C. M. (2025). Recovering carbon black from end-of-life tires: A consequential life cycle assessment. Environmental Impact Assessment Review, 115, 108044. https://doi.org/10.1016/j.eiar.2025.108044

[13] Wei, X., Guo, Z., Zhao, Y., Sun, Y., Hankin, A., & Titirici, M. (2025). Recovery of graphite from industrial lithium-ion battery black mass. RSC Sustainability, 3(1), 264-274. DOI: 10.1039/D4SU00427B

[14] Jiang, G., Pan, J., Deng, W., Sun, Y., Guo, J., Che, K., ... & Zhang, T. (2022). Recovery of high pure pyrolytic carbon black from waste tires by dual acid treatment. Journal of Cleaner Production, 374, 133893. https://doi.org/10.1016/j.jclepro.2022.133893

[15] Bhar, M., Ghosh, S., Krishnamurthy, S., Kaliprasad, Y., & Martha, S. K. (2023). A review on spent lithium-ion battery recycling: from collection to black mass recovery. RSC sustainability, 1(5), 1150-1167. https://doi.org/10.1039/d3su00086a

[16] Searle, S., & Malins, C. (2015). A reassessment of global bioenergy potential in 2050. GCB Bioenergy, 7(2), 328-336. https://doi.org/10.1111/gcbb.12141

[17] Khan, W., Shyamal, D. S., & Kazmi, A. A. (2024). Management of end-of-life tyres in India: current practices, regulatory framework, challenges, and opportunities. Journal of Material Cycles and Waste Management, 26(3), 1310-1325. https://doi.org/10.1007/s10163-024-01937-3

[18] Tian, H., Graczyk-Zajac, M., Kessler, A., Weidenkaff, A., & Riedel, R. (2024). Recycling and reusing of graphite from retired lithium-ion batteries: a review. Advanced Materials, 36(13), 2308494. https://doi.org/10.1002/adma.202308494

[19] World Bioenergy Association. WBA Global Bioenergy Statistics 2018, Summary Report. Available online: https://www.worldbioenergy.org/ (accessed on 10 January 2026).

[20] Mubareka, S. B., Renner, A. (2025). EU Biomass supply, uses, governance and regenerative actions. Publications Office of the European Union. https://data.europa.eu/doi/10.2760/6511190

[21] Camia, A., Cazzaniga, N., Tandetzki, J., Magnolfi, V., & Gurria, P. (2025). Biomass supply and demand in the EU 2012-2022. European Commission, Ispra, JRC143910. Available online: https://publications.jrc.ec.europa.eu/repository/handle/JRC143910 (accessed on 15 January 2026).

[22] Tripathi, N., Hills, C. D., Singh, R. S., & Atkinson, C. J. (2019). Biomass waste utilisation in low-carbon products: harnessing a major potential resource. npj Climate and Atmospheric Science, 2(1), 35. https://doi.org/10.1038/s41612-019-0093-5

[23] Braghiroli, F. L., & Passarini, L. (2020). Valorization of Biomass Residues from Forest Operations and Wood Manufacturing Presents a Wide Range of Sustainable and Innovative Possibilities. Current Forestry Reports, 6(2), 172-183. https://doi.org/10.1007/s40725-020-00112-9

[24] Wang, K., & Tester, J. W. (2023). Sustainable management of unavoidable biomass wastes. Green Energy and Resources, 1(1), 100005. https://doi.org/10.1016/j.gerr.2023.100005

[25] Goldstein Research. (2020). Global Tire Recycling Market Analysis 2025: Opportunity, Demand, Growth and Forecast 2017–2025. https://www.goldsteinresearch.com/report/global-tire-recycling-industry-market-trends-analysis [Accessed 1 May 2026].

[26] Mmereki, D., Machola, B., & Mokokwe, K. (2019). Status of waste tires and management practice in Botswana. Journal of the Air & Waste Management Association, 69(10), 1230-1246. https://doi.org/10.1080/10962247.2017.1279696

[27] Recycled Rubber Coalition. (2024). AN UNEXPECTED ELECTRIC VEHICLE ENVIRONMENTAL PROBLEM WITH COMMON SENSE SOLUTIONS. https://static1.squarespace.com/static/60e7217fc5b6e37824b94aea/t/65afd6639ecc9728992e23ae/1706022503819/EV+White+Paper+Final.pdf [Accessed 4 May 2026].

[28] Czarna-Juszkiewicz, D., Kunecki, P., Cader, J., & Wdowin, M. (2023). Review in Waste Tire Management—Potential Applications in Mitigating Environmental Pollution. Materials, 16(17), 5771. https://doi.org/10.3390/ma16175771

[29] Landi, D., Marconi, M., Gianvincenzi, M., & Mosconi, E. M. (2023). Technical and environmental assessment of a circular economy scenario for end of life tires fibers used as reinforcement in plastic compounds. International Journal on Interactive Design and Manufacturing (IJIDeM), 1-12. https://doi.org/10.1007/s12008-023-01249-0

[30] Czajczyńska, D., Czajka, K., Krzyżyńska, R., & Jouhara, H. (2020). Waste tyre pyrolysis–Impact of the process and its products on the environment. Thermal Science and Engineering Progress, 20, 100690. https://doi.org/10.1016/j.tsep.2020.100690

[31] Paul, S., Rahaman, M., Ghosh, S. K., Katheria, A., Das, T. K., Patel, S., & Das, N. C. (2023). Recycling of waste tire by pyrolysis to recover carbon black: an alternative reinforcing filler. Journal of Material Cycles and Waste Management, 25(3), 1470-1481. https://doi.org/10.1007/s10163-023-01635-6

[32] Urrego-Yepes, W., Cardona-Uribe, N., Vargas-Isaza, C. A., & Martínez, J. D. (2021). Incorporating the recovered carbon black produced in an industrial-scale waste tire pyrolysis plant into a natural rubber formulation. Journal of Environmental Management, 287, 112292. https://doi.org/10.1016/j.jenvman.2021.112292

[33] Paul, S., Rahaman, M., Ghosh, S. K., Katheria, A., Das, T. K., Patel, S., & Das, N. C. (2023). Recycling of waste tire by pyrolysis to recover carbon black: an alternative reinforcing filler. Journal of Material Cycles and Waste Management, 25(3), 1470-1481. https://doi.org/10.1007/s10163-023-01635-6

[34] IEA (2025). Global EV Outlook 2025. IEA. Paris. https://www.iea.org/reports/global-ev-outlook-2025, Licence: CC BY 4.0

[35] Tankou, A., Bieker, G., & Hall, D. (2023). Scaling up reuse and recycling of electric vehicle batteries: Assessing challenges and policy approaches. International Council on Clean Transportation (ICCT). (1-138). https://theicct.org/publication/recycling-electric-vehicle-batteries-feb-23/ [Accessed 5 May 2026]

[36] Biswal, B. K., Zhang, B., Tran, P. T. M., Zhang, J., & Balasubramanian, R. (2024). Recycling of spent lithium-ion batteries for a sustainable future: recent advancements. Chemical Society Reviews, 53(11), 5552-5592. https://doi.org/10.1039/D3CS00898C

[37] Zheng, S., Chen, T., Fang, Y., He, C., Duan, H., Ren, S., & Xu, C. C. (2024). A review of cathode and electrolyte recovery from spent lithium-ion batteries: recent technologies, processes and policies. Resources Chemicals and Materials, 3(3), 188-229. https://doi.org/10.1016/j.recm.2024.01.003

[38] Patnaik, S. (2024). Overview of electrode advances in commercial Li-ion batteries. Ionics, 30(6), 3069-3090. https://doi.org/10.1007/s11581-024-05579-1

[39] Koech, A. K., Mwandila, G., Mulolani, F., & Mwaanga, P. (2024). Lithium-ion battery fundamentals and exploration of cathode materials: A review. South African Journal of Chemical Engineering, 50(1), 321-339. https://doi.org/10.1016/j.sajce.2024.09.008

[40] Chang, L., Yang, W., Cai, K., Bi, X., Wei, A., Yang, R., & Liu, J. (2023). A review on nickel-rich nickel–cobalt–manganese ternary cathode materials LiNi 0.6 Co 0.2 Mn 0.2 O 2 for lithium-ion batteries: performance enhancement by modification. Materials Horizons, 10(11), 4776-4826. https://doi.org/10.1039/D3MH01151H

[41] Zou, Y., Chernyaev, A., Ossama, M., Seisko, S., & Lundström, M. (2024). Leaching of NMC industrial black mass in the presence of LFP. Scientific Reports, 14(1), 10818. https://doi.org/10.1038/s41598-024-61569-3

[42] Tong, Z., Wang, M., Bai, Z., Li, H., & Wang, N. (2025). Advances in lithium-ion battery recycling: Strategies, pathways, and technologies. ChemPhysMater, 4(1), 30-47. https://doi.org/10.1016/j.chphma.2024.05.005

[43] Amalia, D., Singh, P., Zhang, W., & Nikoloski, A. N. (2025). A review of pretreatment methods for spent lithium-ion batteries to produce black mass–comparison of processes of Asia Pacific recyclers. Mineral Processing and Extractive Metallurgy Review, 46(5), 626-643. https://doi.org/10.1080/08827508.2024.2367420

[44] Wei, X., Guo, Z., Zhao, Y., Sun, Y., Hankin, A., & Titirici, M. (2025). Recovery of graphite from industrial lithium-ion battery black mass. RSC Sustainability, 3(1), 264-274. https://doi.org/10.1039/D4SU00427B

[45] Natarajan, S., & Aravindan, V. (2020). An urgent call to spent LIB recycling: whys and wherefores for graphite recovery. Advanced Energy Materials, 10(37), 2002238.

[46] Pajootan, E., Perrin-Sarazin, F., Mateevici, G., Toupin, M., Mihai, O., Methven, B., ... & Chenitz, R. (2025). Second-Life Evaluation of Li-Ion Battery Graphite after Separation and

Pre-and Postpurification Treatments of Black Mass. ACS Sustainable Resource Management, 2(4), 632-641. https://doi.org/10.1021/acssusresmgt.5c00010

[47] Fahad Halim, A. F. M., Poinern, G. E. J., Fawcett, D., Sharma, R., Surendran, S., & R, R. (2025). Biomass-Derived Carbon Nanomaterials: Synthesis and Applications in Textile Wastewater Treatment, Sensors, Energy Storage, and Conversion Technologies. CleanMat, 2(1), 4-58. https://doi.org/10.1002/clem.15

[48] Tian, J., Wang, P., Deng, Z., Wei, D., Chen, H., Zhou, C., ... & Li, L. (2025). Synergistic Dual Heteroatom-Engineered Superactivated Carbon Unlocks Record-High Hydrogen Storage via Mg─F Orbital Hybridization. Advanced Materials, 38(5), e09511. https://doi.org/10.1002/adma.202509511

[49] Serafin, J., & Dziejarski, B. (2024). Activated carbons—preparation, characterization and their application in CO_2 capture: a review. Environmental Science and Pollution Research, 31(28), 40008-40062. https://doi.org/10.1007/s11356-023-28023-9

[50] Dziejarski, B., Serafin, J., Andersson, K., & Krzyżyńska, R. (2023). CO_2 capture materials: a review of current trends and future challenges. Materials Today Sustainability, 24, 100483. https://doi.org/10.1016/j.mtsust.2023.100483

[51] Wang, J., & Kaskel, S. (2012). KOH activation of carbon-based materials for energy storage. Journal of Materials Chemistry, 22(45), 23710-23725. https://doi.org/10.1039/C2JM34066F

[52] Heidarinejad, Z., Dehghani, M. H., Heidari, M., Javedan, G., Ali, I., & Sillanpää, M. (2020). Methods for preparation and activation of activated carbon: a review. Environmental Chemistry Letters, 18, 393-415. https://doi.org/10.1007/s10311-019-00955-0

[53] Azam, K., Shezad, N., Shafiq, I., Akhter, P., Akhtar, F., Jamil, F., Shafigue, S,. Park, Y, K,. & Hussain, M. (2022). A review on activated carbon modifications for the treatment of wastewater containing anionic dyes. Chemosphere, 306, 135566. https://doi.org/10.1016/j.chemosphere.2022.135566

[54] Neolaka, Y. A., Riwu, A. A., Aigbe, U. O., Ukhurebor, K. E., Onyancha, R. B., Darmokoesoemo, H., & Kusuma, H. S. (2023). Potential of activated carbon from various sources as a low-cost adsorbent to remove heavy metals and synthetic dyes. Results in Chemistry, 5, 100711. https://doi.org/10.1016/j.rechem.2022.100711

[55] Nizam, N. U. M., Hanafiah, M. M., Mahmoudi, E., Halim, A. A., & Mohammad, A. W. (2021). The removal of anionic and cationic dyes from an aqueous solution using biomass-based activated carbon. Scientific Reports, 11(1), 1-17. https://doi.org/10.1038/s41598-021-88084-z

[56] Sultana, M., Rownok, M. H., Sabrin, M., Rahaman, M. H., & Alam, S. N. (2022). A review on experimental chemically modified activated carbon to enhance dye and heavy metals adsorption. Cleaner Engineering and Technology, 6, 100382. https://doi.org/10.1016/j.clet.2021.100382

[57] Mariana, M., HPS, A. K., Mistar, E. M., Yahya, E. B., Alfatah, T., Danish, M., & Amayreh, M. (2021). Recent advances in activated carbon modification techniques for enhanced heavy metal adsorption. Journal of Water Process Engineering, 43, 102221. https://doi.org/10.1016/j.jwpe.2021.102221

[58] Shahrokhi-Shahraki, R., Benally, C., El-Din, M. G., & Park, J. (2021). High efficiency removal of heavy metals using tire-derived activated carbon vs commercial activated carbon: Insights into the adsorption mechanisms. Chemosphere, 264, 128455. https://doi.org/10.1016/j.chemosphere.2020.128455

[59] Xie, B., Qin, J., Wang, S., Li, X., Sun, H., & Chen, W. (2020). Adsorption of phenol on commercial activated carbons: modelling and interpretation. International Journal of Environmental Research and Public Health, 17(3), 789. https://doi.org/10.3390/ijerph17030789

[60] Reza, M. S., Yun, C. S., Afroze, S., Radenahmad, N., Bakar, M. S. A., Saidur, R., Taweekun, J., & Azad, A. K. (2020). Preparation of activated carbon from biomass and its' applications in water and gas purification, a review. Arab Journal of Basic and Applied Sciences, 27(1), 208-238. https://doi.org/10.1080/25765299.2020.1766799

[61] El-Bery, H. M., Saleh, M., El-Gendy, R. A., Saleh, M. R., & Thabet, S. M. (2022). High adsorption capacity of phenol and methylene blue using activated carbon derived from lignocellulosic agriculture wastes. Scientific Reports, 12(1), 5499. https://doi.org/10.1038/s41598-022-09475-4

[62] Sathishkumar, R., & Prakash, R. (2026). A review on activated carbons (AC) for CO_2 capture applications: preparation, characterization and surface modification methods. Fuel, 405, 136521. https://doi.org/10.1016/j.fuel.2025.136521

[63] Umar, M., Yusuf, B. O., Aliyu, M., Hussain, I., Alhassan, A. M., Awad, M. M., ... & Ganiyu, S. A. (2025). Advancing frontiers in CO_2 capture: The renaissance of biomass-derived carbon materials. Coordination Chemistry Reviews, 526, 216380. https://doi.org/10.1016/j.ccr.2024.216380

[64] Sawalha, H., Maghalseh, M., Qutaina, J., Junaidi, K., & Rene, E. R. (2020). Removal of hydrogen sulfide from biogas using activated carbon synthesized from different locally available biomass wastes-a case study from Palestine. Bioengineered, 11(1), 607-618. https://doi.org/10.1080/21655979.2020.1768736

[65] Wang, S., Nam, H., & Nam, H. (2020). Preparation of activated carbon from peanut shell with KOH activation and its application for H2S adsorption in confined space. Journal of Environmental Chemical Engineering, 8(2), 103683. https://doi.org/10.1016/j.jece.2020.103683

[66] Chan, Y. H., Lock, S. S. M., Wong, M. K., Yiin, C. L., Loy, A. C. M., Cheah, K. W., Chai, S. Y. W., Li, C., How, B. S., Chin, B. L. F., Chan, Z. P., & Lam, S. S. (2022). A state-of-the-art review on capture and separation of hazardous hydrogen sulfide (H2S): Recent advances, challenges and outlook. Environmental Pollution, 314, 120219. https://doi.org/10.1016/j.envpol.2022.120219

[67] Hanif, M. A., Ibrahim, N., & Abdul Jalil, A. (2020). Sulfur dioxide removal: An overview of regenerative flue gas desulfurization and factors affecting desulfurization capacity and sorbent regeneration. Environmental Science and Pollution Research, 27(22), 27515-27540. https://doi.org/10.1007/s11356-020-09191-4

[68] Wang, L., Sha, L., Zhang, S., Cao, F., Ren, X., & Levendis, Y. A. (2022). Preparation of activated coke by carbonization, activation, ammonization and thermal treatment of sewage sludge and waste biomass for SO_2 absorption applications. Fuel Processing Technology, 231, 107233. https://doi.org/10.1016/j.fuproc.2022.107233

[69] Jacobs, J. H., Chou, N., Lesage, K. L., Xiao, Y., Hill, J. M., & Marriott, R. A. (2023). Investigating activated carbons for SO_2 adsorption in wet flue gas. Fuel, 353, 129239. https://doi.org/10.1016/j.fuel.2023.129239

[70] Li, Q., Hou, Y., Xiang, N., Liu, Y., & Huang, Z. (2020). A new insight into the promotional effect of nitrogen-doping in activated carbon for selective catalytic reduction of NO_x with NH_3.

Science of the Total Environment, 740, 140158. https://doi.org/10.1016/j.scitotenv.2020.140158

[71] Niu, J., Zhang, H., Li, L., & Guo, Y. (2021). Cost-effective activated carbon (AC) production from partial substitution of coal with red mud (RM) as additive for SO_2 and NO_x abatement at low temperature. Fuel, 293, 120448. https://doi.org/10.1016/j.fuel.2021.120448

[72] Park, B., & Choi, Y. C. (2022). Evaluation of NO_x removal performance of foam composites with titanium dioxide and active carbon. Construction and Building Materials, 348, 128646. https://doi.org/10.1016/j.conbuildmat.2022.128646

[73] Ma, X., Yang, L., & Wu, H. (2021). Removal of volatile organic compounds from the coal-fired flue gas by adsorption on activated carbon. Journal of Cleaner Production, 302, 126925. https://doi.org/10.1016/j.jclepro.2021.126925

[74] Li, X., Zhang, L., Yang, Z., Wang, P., Yan, Y., & Ran, J. (2020). Adsorption materials for volatile organic compounds (VOCs) and the key factors for VOCs adsorption process: A review. Separation and Purification Technology, 235, 116213. https://doi.org/10.1016/j.seppur.2019.116213

[75] Isinkaralar, K. (2024). Multi-component volatile organic compounds (VOCs) treatment nexus: High-performance of activated carbon derived from residual agroforestry biomass. International Journal of Environmental Science and Technology, 21(1), 925-938. https://doi.org/10.1007/s13762-023-05202-2

[76] Rouquerol, J., Rouquerol, F., Llewellyn, P., Maurin, G., & Sing, K. (2012). Adsorption by Powders and Porous Solids: Principles, Methodology and Applications. Academic Press. https://doi.org/10.1016/C2010-0-66232-8.

[77] Yang, R. T. (1997). Gas Separation by Adsorption Processes, Series on Chemical Engineering, (Vol. 1). Imperial College Press. https://doi.org/10.1142/p037.

[78] García–Nieto, P. J., García–Gonzalo, E., & Paredes–Sánchez, J. P. (2024). Estimation of the coal higher heating value for energy systems relied on ultimate analysis with machine learning techniques. Fuel, 357, 130037. https://doi.org/10.1016/j.fuel.2023.130037

[79] Cychosz, K. A., & Thommes, M. (2018). Progress in the physisorption characterization of nanoporous gas storage materials. Engineering, 4(4), 559-566. https://doi.org/10.1016/j.eng.2018.06.001

[80] Thommes, M., Morlay, C., Ahmad, R., & Joly, J. P. (2011). Assessing surface chemistry and pore structure of active carbons by a combination of physisorption (H_2O, Ar, N_2, CO_2), XPS and TPD-MS. Adsorption, 17(3), 653-661. https://doi.org/10.1007/s10450-011-9360-4

[81] Wang, Y., Hu, X., Guo, T., Hao, J., Si, C., & Guo, Q. (2021). Efficient CO_2 adsorption and mechanism on nitrogen-doped porous carbons. Frontiers of Chemical Science and Engineering, 15, 493-504. https://doi.org/10.1007/s11705-020-1967-0

[82] Dombrowski, R. J., Hyduke, D. R., & Lastoskie, C. M. (2000). Pore size analysis of activated carbons from argon and nitrogen porosimetry using density functional theory. Langmuir, 16(11), 5041-5050. https://doi.org/10.1021/la990827a

[83] Song, Z. Z., Abula, A., Zhao, J. Y., Liu, G. D., Li, M. R., Yang, D. L., & Wang, Y. L. (2022). A novel hybrid thermodynamic model for pore size distribution characterisation for shale. Petroleum Science, 19(3), 963-978. https://doi.org/10.1016/j.petsci.2021.12.015

[84] Bhargava, R., & Levin, I. W. (2005). Fourier Transform Mid-infrared Spectroscopic Imaging: Microspectroscopy with Multichannel Detectors. Spectrochemical Analysis Using Infrared Multichannel Detectors, 1-24. DOI:10.1002/9780470988541

[85] Peticolas, W. L. (1972). Inelastic light scattering and the Raman effect. Annual Review of Physical Chemistry, 23(1), 93-116. https://doi.org/10.1146/annurev.pc.23.100172.000521

[86] Smith, E., & Dent, G. (2019). Modern Raman spectroscopy: a practical approach. John Wiley & Sons. DOI:10.1002/0470011831

[87] Zhou, W., Apkarian, R., Wang, Z. L., & Joy, D. (2007). Fundamentals of scanning electron microscopy (SEM). Scanning microscopy for nanotechnology: techniques and applications, 1-40. https://doi.org/10.1007/978-0-387-39620-0

[88] Bunaciu, A. A., UdriŞTioiu, E. G., & Aboul-Enein, H. Y. (2015). X-ray diffraction: instrumentation and applications. Critical Reviews in Analytical Chemistry, 45(4), 289-299. https://doi.org/10.1080/10408347.2014.949616

[89] Bubert, H., Rivière, J. C., & Werner, W. S. (2011). X-Ray Photoelectron Spectroscopy (XPS). Surface and Thin Film Analysis: A Compendium of Principles, Instrumentation, and Applications, 7-41. DOI:10.1002/9783527636921

[90] Zheng, Y., Wang, J., Li, D., Liu, C., Lu, Y., Lin, X., & Zheng, Z. (2021). Insight into the KOH/$KMnO_4$ activation mechanism of oxygen-enriched hierarchical porous biochar derived

from biomass waste by in-situ pyrolysis for methylene blue enhanced adsorption. Journal of Analytical and Applied Pyrolysis, 158, 105269. https://doi.org/10.1016/j.jaap.2021.105269

[91] Chen, Y. D., Chen, W. Q., Huang, B., & Huang, M. J. (2013). Process optimization of $K_2C_2O_4$-activated carbon from kenaf core using Box–Behnken design. Chemical Engineering Research and Design, 91(9), 1783-1789. https://doi.org/10.1016/j.cherd.2013.02.024